2017

Crop evapotranspiration calculation using infrared thermometers aboard center pivots

Paul D. Colaizzi
USDA-ARS, Paul.Colaizzi@ARS.USDA.GOV

Susan A. O'Shaughnessy
USDA-ARS, Susan.OShaughnessy@ars.usda.gov

Steven R. Evett
USDA-ARS, steve.evett@ars.usda.gov

Ryan B. Mounce
USDA-ARS

Agricultural Water Management 187 (2017) 173–189

Contents lists available at ScienceDirect

Agricultural Water Management

journal homepage: www.elsevier.com/locate/agwat

Research Paper

Crop evapotranspiration calculation using infrared thermometers aboard center pivots

Paul D. Colaizzi[a,*], Susan A. O'Shaughnessy[a], Steve R. Evett[a], Ryan B. Mounce[b]

[a] USDA Agricultural Research Service, Conservation and Production Research Laboratory, P.O. Drawer 10, 2300 Experiment Station Road, Bushland, TX 79012, USA

[b] USDA Agricultural Research Service, Cropping Systems Research Laboratory, 3810 4th Street, Lubbock, TX 79415, USA

ARTICLE INFO

Article history:
Received 19 September 2016
Received in revised form 9 March 2017
Accepted 10 March 2017
Available online 27 March 2017

Keywords:
Two source energy balance model
Soil water balance
Remote sensing
Texas

ABSTRACT

Irrigation scheduling using remotely sensed surface temperature can result in equal or greater crop yield and crop water use efficiency compared with irrigation scheduling using in-situ soil water profile measurements. Crop evapotranspiration (*ETc*) is useful for irrigation scheduling, and can be calculated using surface temperature. Recent advances in wireless infrared thermometers (IRTs) have made surface temperature measurement a viable alternative to in-situ soil water profile measurements, and wireless IRTs are practical for deployment aboard moving irrigation systems, such as center pivots. However, *ETc* calculation has not been tested using IRTs aboard center pivots in conjunction with recent advances in a two-source energy balance (TSEB) model. We compared daily *ETc* calculated by a TSEB model to daily *ETc* estimated by a simple soil water balance (SSWB), where the SSWB used volumetric soil water measured by a field calibrated neutron probe to the 2.4-m depth. Crops included two seasons each of corn (*Zea mays* L.), cotton (*Gossypium hirsutum* L.), and grain sorghum (*Sorghum bicolor* L.) at Bushland, Texas, USA. Discrepancies of TSEB vs. SSWB daily *ETc* were similar for each crop and season, and had root mean squared error from 1.5 to 1.8 mm per day, mean absolute error from 1.1 to 1.5 mm per day, and mean bias error from −0.51 to 0.63 mm per day. A sensitivity analysis was conducted for daily evaporation (*E*), daily transpiration (*T*), and *ETc* calculated by the TSEB model. These were most sensitive to radiometric surface temperature, air temperature, the reference temperature used in time scaling (i.e., to convert instantaneous to daily *E*, *T*, and *ETc*), and incoming solar irradiance. Because over half of the irrigated area in the USA is now by center pivot, *ETc* calculated using IRTs aboard center pivots will be useful to maintain or increase crop water productivity.

Published by Elsevier B.V.

1. Introduction

In-field quantification of crop evapotranspiration (*ETc*) and water stress will play an increasing role in managing and enhancing crop water productivity (Ahmad et al., 2009; Evans and Sadler, 2008; Senay et al., 2009; Zwart and Bastiaanssen, 2007). Specific applications include irrigation scheduling and irrigation automation (Jones, 2004; O'Shaughnessy et al., 2015; Osroosh et al., 2015); additional applications include detection and mitigation of abiotic and biotic stresses, which may be caused by malfunctioning irrigation equipment, salinity or other soil and water constituents inhibiting crop economic yield, pests, and disease (Falkenberg et al., 2007; Li et al., 2008). Numerous methods exist for estimating *ETc*, including the crop coefficient-reference evapotranspiration approach (Allen et al., 1998; Anderson et al., 2017; Howell et al., 2004; Hunsaker et al., 2005), lysimetry (Howell et al., 1995, 1997), boundary layer measurements (Bowen ratio, eddy covariance, scintillometry, surface renewal; Alfieri et al., 2012; French et al., 2012; Liu et al., 2011; Todd et al., 2000), in-situ soil water profile measurement (Evett et al., 2012), and radiometric canopy temperature measurement (Maes and Steppe, 2012). The latter is derived from, or assumed equal to, remotely sensed directional brightness temperature of vegetated surfaces (Norman and Becker, 1995). Routine estimates of *ETc* using canopy temperature measurements have several practical advantages compared with alternative methods. Also, many forms of water stress indices used in irrigation scheduling or to detect abiotic or biotic stress are based on actual *ETc* relative to a non-water stressed *ETc* value, where actual *ETc* is estimated by in-field canopy temperature measurements (Jackson, 1982; Moran et al., 1994; Jones, 2004).

* Corresponding author.
E-mail address: Paul.Colaizzi@ars.usda.gov (P.D. Colaizzi).

http://dx.doi.org/10.1016/j.agwat.2017.03.016
0378-3774/Published by Elsevier B.V.

The advantages of using canopy temperature to estimate *ETc* are at once the result of, and contingent on, meeting certain requirements of real-time farm management (Jackson, 1984). These include spatial resolution (several meters), repeat frequency (no more than a few days), and turnaround time (interval from field measurement to useful data product; no more than a few minutes). These are in addition to the obvious requirements of reasonable instrument cost, precision, accuracy, and extent of field area coverage. The recent development of unmanned aerial vehicles (UAVs) have overcome many technical barriers to meeting these requirements (Bellvert et al., 2014; Berni et al., 2009; Gago et al., 2015; Zarco-Tejada et al., 2013), but regulatory barriers may restrict UAVs from flying in certain areas (Thomasson et al., 2016; Woldt et al., 2015). Moving irrigation systems have long been recognized as a possible platform for ground-based radiometers, particularly infrared thermometers (IRTs) used to measure canopy temperature (Phene et al., 1985; Sadler et al., 2002). Center pivots now occupy over 50% and 80% of the irrigated area in the USA and US Great Plains, respectively (USDA, 2014). Their widespread adoption, along with proper design, installation, and management, offer unprecedented opportunity to increase crop water productivity, but nonetheless represent a primary consumer of freshwater resources (Moore et al., 2015). Center pivot rotational speeds can be managed where angular positions of sprinklers are distributed to different times of the day. This is intended to improve irrigation distribution uniformity over the season by distributing daytime and nighttime differences in evaporative and wind drift losses more uniformly throughout the field (Han et al., 1994; Playán et al., 2005; Steiner et al., 1983). This can also distribute midday and afternoon coverage of IRTs (when *ETc* typically reaches diurnal maxima) to all angular positions of the field, albeit there is a tradeoff between field coverage and repeat frequency (Haberland et al., 2010).

Irrigation scheduling can be automated using canopy temperature measured by stationary IRTs (Evett et al., 2000; Upchurch et al., 1996; Wanjura et al., 1992). The concept was extended to moving IRTs aboard center pivots, and resulted in crop yield and water use efficiency comparable or greater than manual irrigation scheduling using soil water profile measurements by a neutron probe (O'Shaughnessy and Evett, 2010a; O'Shaughnessy et al., 2012a, 2013; Peters and Evett, 2008). The canopy temperature-based algorithms used in these studies included the time-temperature threshold (Wanjura et al., 1992), crop water stress index (Jackson et al., 1981), and an integrated crop water stress index (O'Shaughnessy et al., 2012a). These algorithms do not distinguish between soil and canopy temperature, which can differ by more than 30 °C, and can influence the apparent surface temperature during partial canopy cover. This has sometimes resulted in unneeded irrigation events occurring early in the season prior to full canopy cover (O'Shaughnessy et al., 2011a,b).

A two-source energy balance (TSEB) model may provide a way to reduce errors in *ETc* and crop water stress calculations by partitioning surface temperature into soil and canopy components. The TSEB model of Norman et al. (1995) and Kustas and Norman (1999) uses directional brightness surface temperature, does not require much greater input data compared with the theoretical crop water stress index, and solves the energy balance of the soil and canopy regimes separately. In addition to calculating the soil and canopy temperature components, the TSEB calculates soil evaporation (*E*) and canopy transpiration (*T*), which can be combined as *ETc*. Previous studies tested the TSEB for corn and soybean in Central Iowa (USA) with partial to full canopy cover (Anderson et al., 2005; Li et al., 2005). In Bushland, Texas (USA), which is a semiarid climate noted for large advected sensible heat flux, the TSEB model was shown to calculate *ETc* and latent heat flux for fully irrigated cotton with relatively small discrepancies (<20%) compared with *ETc* measured by lysimeters and eddy covariance, respectively (Anderson et al., 2012; Cammalleria et al., 2014; Kustas et al., 2012). Recent studies also improved *E* and *T* partitioning, along with *ETc* calculations, for the fully irrigated cotton at that study location (Colaizzi et al., 2016a; Song et al., 2016). These studies used stationary wired IRTs and stationary inverted pyrgeometers at 15-min intervals and small spatial scales, and one-time-of-day satellite measurements at larger spatial scales. However, no TSEB model version has been tested for moving IRTs aboard center pivots, and relatively few TSEB studies have considered different crops grown over multiple seasons, which entail relatively wide ranges of climatic and growing conditions typical of the Southern High Plains region of the USA (Baumhardt et al., 2016). Further, the recent TSEB model version has not been tested using recently developed wireless IRTs and wireless sensor networks (O'Shaughnessy and Evett, 2010b; O'Shaughnessy et al., 2011b).

The objective of this study was to test the TSEB model in calculating *ETc* using moving IRTs aboard center pivots. A secondary objective was to conduct a sensitivity analysis of *E*, *T*, and *ETc* to selected input variables (likely as having the most uncertainty in practice) for a small, medium, and large canopy. Although separate *E* or *T* measurements were presently not available in the center pivot fields, their inclusion in the sensitivity analysis was deemed important in assessing the impact of different canopy sizes. A forthcoming paper will extend the TSEB model to include thermal-based indices for irrigation scheduling, and compare these to existing indices.

2. Materials and methods

2.1. TSEB model overview

The TSEB model version used here was described in Colaizzi et al. (2016a). This was essentially the series resistance TSEB version described by Norman et al. (1995) and Kustas and Norman (1999) with several modifications designed for ground based IRTs and row crops. The series resistance formulation was chosen over the parallel resistance alternative because the former was shown to be less sensitive to input variables over a wider range of vegetation cover (Li et al., 2005). The modifications included submodels to calculate the vegetation view factor in an IRT footprint (Colaizzi et al., 2010), partitioning net shortwave and net longwave radiation to the soil and canopy components (Colaizzi et al., 2012a,b), calculation of surface soil heat flux in crop interrows (Colaizzi et al., 2016b,c), replacing the Priestley-Taylor with the Penman-Monteith equation to calculate initial crop transpiration (Colaizzi et al., 2012c, 2014, 2016a), and calculation of daily *ETc* from one-time-of-day IRT measurements by the time scaling method (Peters and Evett, 2004). In addition, leaf area index (*LAI*) is a required input throughout the TSEB model. However, only canopy width (w_C), canopy height (h_C), and plant population measurements were available in the present study, and *LAI* measurements were available only in a few seasons and in a limited number of plots. Therefore, *LAI* was estimated by an allometric method that used plant population, h_C, and cumulative growing degree days (Colaizzi et al., 2017).

The TSEB model with series resistance includes an aerodynamic resistance (r_A), canopy boundary layer resistance (r_X), and soil surface resistance (Fig. 1). Sensible heat fluxes (*H*) are transferred through these resistances by temperature gradients, and are related to available energy and latent heat fluxes (*LE*) by

$$LE = R_N - G_0 - H \quad (1)$$

where R_N is net radiation, G_0 is surface soil heat flux, and all terms have $W\,m^{-2}$ units. In this sign convention, R_N is positive towards the canopy, and all other terms are positive away from the canopy.

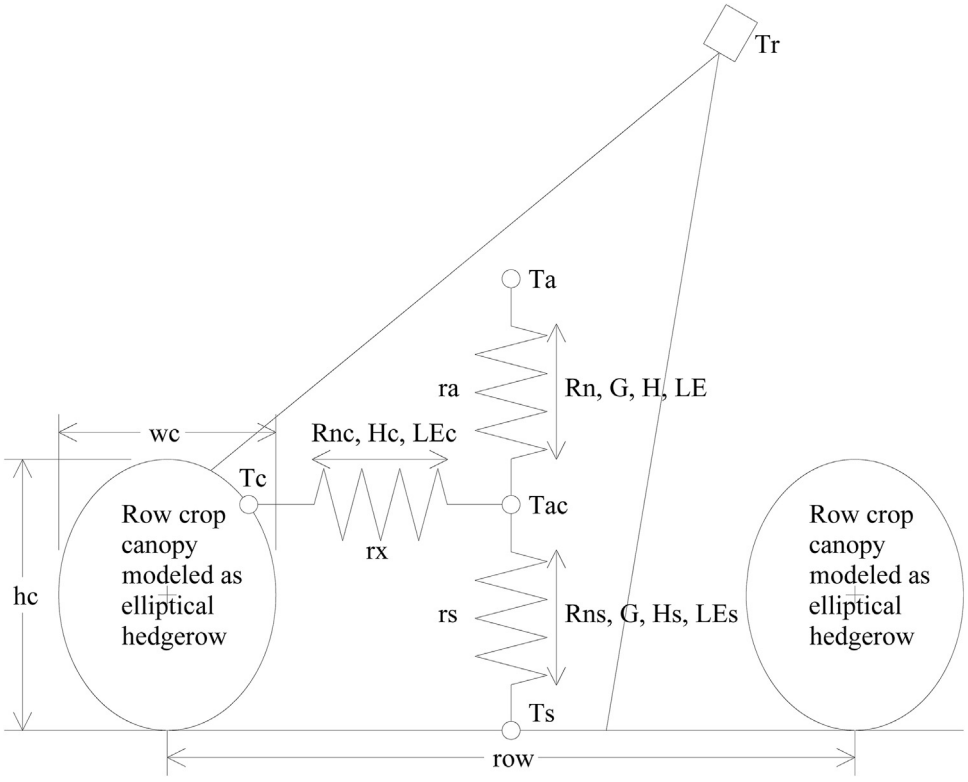

Fig. 1. Two source energy balance (TSEB) model with series resistances (Norman et al., 1995; Colaizzi et al., 2016a). See TSEB Model Overview section for definition of symbols.

The energy balance can be partitioned to the soil and canopy components as:

$$LE_C = R_{N,C} - H_C \tag{2a}$$

$$LE_S = R_{N,S} - G_0 - H_S \tag{2b}$$

where the subscripts C and S stand for canopy and soil, respectively. The sensible heat flux terms were calculated as:

$$H = \rho C_P \frac{T_{AC} - T_A}{r_A} \tag{3a}$$

$$H_C = \rho C_P \frac{T_C - T_{AC}}{r_X} \tag{3b}$$

$$H_S = \rho C_P \frac{T_S - T_{AC}}{r_S} \tag{3c}$$

where ρ is the density of moist air (kg m^{-3}), C_P is the specific heat of air (1013 J kg^{-1} K^{-1}), T_C, T_A, T_S, and T_{AC} are the temperatures of the canopy, air, soil, and air temperature within the canopy boundary layer, respectively (K),and all other terms were as defined previously. The resistance terms were calculated following Norman et al. (1995) and Kustas and Norman (1999), which generally apply to row crops planted in uniform soil and under conventional tillage (but may not apply to natural vegetation with non-cultivated or rocky soil; e.g., Morillas et al., 2013; Kustas et al., 2016).

Radiometric surface temperature (T_R) is related to T_C and T_S by:

$$\varepsilon T_R^4 = f_{VR}\varepsilon_C T_C^4 + (1 - f_{VR})\varepsilon_S T_S^4 \tag{4}$$

where ε is the composite surface emissivity, and f_{VR} is the vegetation view factor in an IRT footprint (Colaizzi et al., 2010), and T_R was calculated from the directional brightness temperature (T_B) reported by an IRT (i.e., corrected for surface emissivity and reflected hemispherical longwave atmospheric irradiance; Norman and Becker, 1995):

$$T_R^4 = \frac{\varepsilon_R}{\varepsilon} T_B^4 + \left(1 - \frac{1}{\varepsilon}\right) \varepsilon_{atm} T_A^4 \tag{5}$$

where ε_R is the target emissivity that is set in the IRT firmware, ε_{atm} is the hemispherical longwave atmospheric emissivity (Idso, 1981), and all other terms are as defined previously. Idso et al. (1969) and Campbell and Norman (1998) showed that $\varepsilon_C \sim 0.98$ for most agricultural crops (although for a deep canopy, effective ε_C can increase to ~0.99 due to multiple reflections of longwave radiation inside the canopy). Field measurements of ε_S over bare soil at the study location were obtained by a Cimel CE 312 multiband thermal radiometer (Cimel Electronique, Paris, France), and $\varepsilon_S = 0.98 \pm 0.01$. This supported the assumption of $\varepsilon = \varepsilon_C = \varepsilon_S = 0.98$.

The system of equations was solved using a secant method (Norman et al., 1995), which was slightly modified for the Penman-Monteith TSEB version (Colaizzi et al., 2012c, 2016a). LE was converted to crop evapotranspiration (ETc) by:

$$ET_C = LE \frac{1000\tau_i}{10^6 \rho_W \lambda} \tag{6}$$

where 1000 converts m to mm, τ_i is the desired time interval (900 s), 10^6 converts MJ to J, ρ_W is the density of water (assumed 1000 kg m^{-3} at 20 °C), and λ is the latent heat of vaporization, and $\lambda \sim 2.44$ MJ kg^{-1}.

Since T_B was measured by IRT arrays on a moving center pivot, T_B was available at only one time or a few times of day for any point location. Therefore, following conversion from T_B to T_R, the time scaling method of Peters and Evett (2004) calculated T_R for each 15-min interval over 24 h:

$$T_{R,t2} = T_E + \frac{\left(T_{R,t1} - T_E\right)\left(T_{REF,t2} - T_E\right)}{\left(T_{REF,t1} - T_E\right)} \tag{7}$$

where T_{REF} is a reference temperature, T_E is the daily minimum T_{REF}, t_1 is the time of the one-time-of-day T_R measurement, and t_2 is all other times of day over 24 h. Here, T_{REF} was measured by stationary IRTs at the study location and averaged to 15-min intervals, or was calculated for a non-water stressed crop (Jackson et al., 1981) if T_{REF} measurements were missing (care should be exercised to avoid mixing T_{REF} sources within a 24 h interval; i.e., midnight to midnight). Only T_R data were used when the solar zenith angle <80°; the time scaling method was not accurate for T_R within 1–2 h of dawn or dusk (Peters and Evett, 2004). With diurnal T_R calculated, the TSEB model was run for each 15-min interval, and 15-min *ETc* were summed to daily (24 h) *ETc*.

2.2. Study location

All data reported here were obtained at the USDA Agricultural Research Service Conservation and Production Research Laboratory, Bushland, Texas, USA (35° 11′ N, 102° 6′ W, 1170 m above MSL). The climate is semiarid with mean annual precipitation of 470 mm and mean Class A pan evaporation of 2600 mm, and regional and local advection is common. Soils are classed as Pullman clay loam (fine, mixed, superactive, thermic Torrertic Paleustoll) consisting of three primary layers, including an Ap horizon (0 to ~0.3 m), a Bt horizon with relatively high clay content (~0.3–1.3 m), and a Btk horizon with high calcic content (>1.3 m) (USDA-NRCS, 2016). The Pullman clay loam has slow permeability and a plant available water content of approximately 140 mm m^{-1} (Evett et al., 2012; Tolk and Evett, 2012).

2.3. Soil water balance

A simple soil water balance (SSWB) was used to estimate *ETc*, which served as ground-truth to test the TSEB model in calculating *ETc*. A general form of the soil water balance is:

$$ET_C = I + P + F + R + \Delta S \tag{8}$$

where I is irrigation, P is precipitation, F is net subsurface flux into the control volume, R is net runoff or runon to the control volume surface, and ΔS is the net change in soil water stored in the control volume (all have mm units). Here, F can include horizontal and vertical fluxes. Evett et al. (2012) compared three variants of the soil water balance to *ETc* measured by weighing lysimeters, including the SSWB (where F was assumed equal to zero), the SSWB but with vertical F calculated at the bottom of the control volume having a fixed depth (2.4-m depth, which was the extent of volumetric soil water measurements by neutron probe), and with vertical F calculated at the bottom of the control volume defined by the zero flux plane. All three variants assumed horizontal F and R were zero, which was justified by uniform soil having slopes less than 0.0025 m m^{-1}, uniform irrigation, and use of furrow dikes and raised beds to minimize surface movement of I and P (Schneider and Howell, 2000). Inclusion of vertical F reduced *ETc* by approximately 0.1 mm d^{-1} (except during heavy rain later in the season when vertical F was larger), and all three methods did not differ substantially when compared with *ETc* measured by weighing lysimeters. Therefore, the SSWB method was used in the present study, making the assumption that $F = R = 0$.

Volumetric soil water was measured by a field calibrated neutron probe on successive days to determine ΔS. Field calibration procedures were described in Evett, (2008), and resulted in agreement better than 0.01 m^3 m^{-3} when compared with independent gravimetric soil samples obtained with a Madera probe (Precision Machine, Inc., Lincoln, Neb.). Separate calibrations were obtained for each soil horizon (Ap, Bt, and Btk) over the range of possible volumetric soil water contents. Volumetric soil water was measured in electrical metallic access tubes, where a single tube was installed in the center of each experimental plot used in the present study (described later). Measurements were obtained from 0.1- to 2.3-m depths in 0.2-m increments, which ensured that the complete profile was measured down to 2.4 m because the sphere diameter of emitted neutrons is typically ≥ 0.2 m in the Pullman soil. The 2.4-m depth was well below the rooting depths of crops grown in the region, and would detect any vertical or horizontal F within this control volume. Measurement depths relative to the surface were controlled and standard readings were obtained using a depth control stand (Evett et al., 2003). The depth control stand was critical to maintain accuracy of measurements near the surface (<0.3 m), which are very sensitive to the probe depth.

The frequency of neutron probe measurements varied but was weekly or biweekly for plots having the largest irrigation rates, and less frequent for plots having more deficit irrigation rates. Therefore, *ETc* estimated by the SSWB spanned varying numbers of days. However, numerous previous studies have reported *ETc* at daily (24 h) intervals (e.g., Cammalleria et al., 2014; French et al., 2007, 2015; Song et al., 2016). Hence it was desired to interpolate *ETc* to daily intervals between neutron probe measurement days to facilitate comparison. This was accomplished using a single crop coefficient and reference evapotranspiration approach. Cumulative reference evapotranspiration was calculated during the interval of successive neutron probe measurements. The single crop coefficient (Kc) was then calculated as

$$K_C = \frac{ET_C}{\sum_{d=1}^{n} ET_{O,d}} \tag{9}$$

where *ETc* was calculated by the SSWB (mm), *ETo* is the ASCE Standardized Penman-Monteith ET equation for a short reference crop at daily intervals (mm) (ASCE, 2005), and n is the number of days between successive neutron probe measurements. Note that ETc and hence Kc were specific to each neutron tube or experimental plot. Then Kc was interpolated to daily intervals by fitting a Fourier series function (Slack et al., 1996):

$$K_C = a_0 + \sum_{f=1}^{F} \left(a_f \sin\theta_f + b_f \cos\theta_f \right) \tag{10}$$

and

$$\theta_f = 2\pi f \frac{CGDD}{CGDD_{max}} \tag{11}$$

where a_0, $a_1 \ldots a_F$, and $b_1 \ldots b_F$ are fit constants, f is the order of the Fourier series ($f = 1$ because higher orders were not significant), *CGDD* is cumulative growing degree days of the crop since planting (°C), and $CGDD_{\max}$ is the maximum cumulative growing degree days (i.e., from planting to harvest or maturity) (°C). The *CGDD* were calculated following McMaster and Wilhelm (1997) as:

$$CGDD = \sum_{d=1}^{D} \left(T_{\overline{A}} - T_{base} \right)_d \tag{12}$$

where d is the number of days since planting, D is the number of days elapsed at $CGDD_{max}$, $T_{\overline{A}}$ is the mean daily air temperature, and T_{base} is the crop base temperature (i.e., below which no crop growth or development occurs), and $T_{\overline{A}}$ is constrained by:

$$T_{\overline{A}} = \left(T_{A,max} + T_{A,min} \right) / 2 \quad for T_{A,max} \le T_{peak} \text{ and } T_{A,min} \ge T_{base} \tag{13a}$$

$$T_{\overline{A}} = \left(T_{peak} + T_{A,min} \right) / 2 \quad for T_{A,max} \ge T_{peak} \text{ and } T_{A,min} \ge T_{base} \tag{13b}$$

$$T_{\overline{A}} = \left(T_{A,max} + T_{base} \right) / 2 \quad for T_{A,max} \le T_{peak} \text{ and } T_{A,min} \le T_{base} \tag{13c}$$

$$T_{\overline{A}} = T_{base} \quad for T_{A,max} \le T_{base} \text{ and } T_{A,min} \le T_{base} \tag{13d}$$

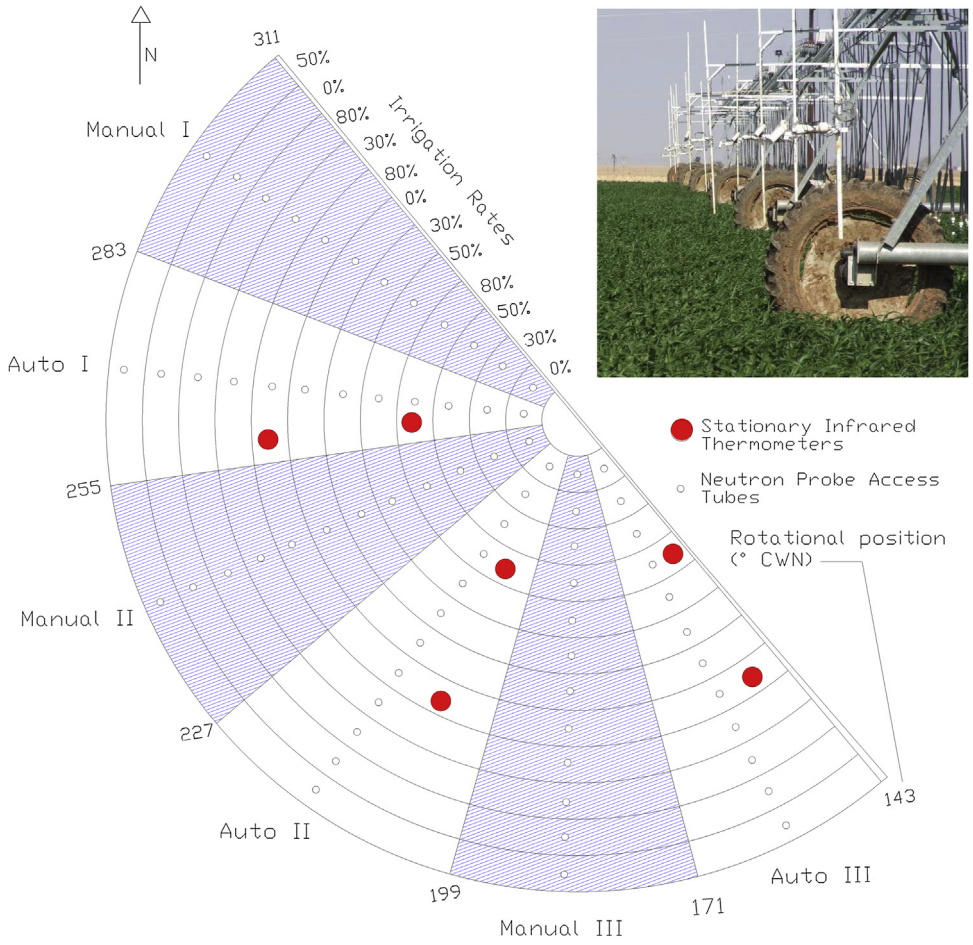

Fig. 2. Photograph showing wireless infrared thermometers aboard a center pivot, and experimental plan example for the South Center Pivot (S PVT), 2011 sorghum season, including irrigation rates, irrigation scheduling treatments (Manual by neutron probe or automatic [Auto] by infrared thermometers), locations of stationary infrared thermometers, neutron probe access tubes. Adopted from O'Shaughnessy et al. (2013).

$$T_{\overline{A}} = \left(T_{peak} + T_{base}\right)/2 \quad for T_{A,max} > T_{peak} \text{ and } T_{A,min} < T_{base} \quad (13e)$$

where $T_{A,max}$ is the maximum daily air temperature, $T_{A,min}$ is the minimum daily air temperature, and T_{peak} is the crop peak development temperatures (i.e., above which no increase in rate of crop growth or development occurs), and all temperature variables have (°C) units. Crops used the present study included corn, cotton, and grain sorghum and are further described in the next section. Here, values of T_{base} and T_{peak} used were 10 °C and 30 °C, respectively, for corn (Gilmore and Rogers, 1958); 15 °C and 50 °C, respectively, for cotton (Peng et al., 1989), and 10 °C and 38 °C, respectively, for grain sorghum (Gerik et al., 2003).

The SSWB approach was tested by comparing daily *ETc* by the SSWB and fit Kc functions to daily *ETc* measured by weighing lysimeters using a separate dataset previously published by Evett et al. (2012). Briefly, these data included two 4.7-ha fields planted in cotton in 2008. Large monolithic weighing lysimeters were located in the centers of each field (designated NE and SE for Northeast and Southeast, respectively). Both fields were planted in raised beds and furrow diked following crop establishment, and fully irrigated by sprinkler. Row orientations were north-south for the NE field and east-west for the SE field. Each field contained eight neutron access tubes, with six outside and two inside each lysimeter. The same procedure was used as described above for neutron probe calibration and measurements for the six tubes outside the lysimeters. Data from that study were used because *ETc* from SSWB vs. lysimeters were already compared at intervals between neutron measurement days, but not daily intervals that required interpolation by fitting Kc functions as shown here.

2.4. Additional field measurements

Measurements used to calculate daily *ETc* using the TSEB model and SSWB method were obtained in two center pivot fields (e.g., Fig. 2) and at a micrometeorological station. The two center pivot fields were located approximately 1.6 km north and south relative to each other, and were designated as North Pivot (N PVT) and South Pivot (S PVT). The N PVT included three spans and the S PVT included six spans with approximately 45-m lengths, resulting in ~5.7- and 23-ha irrigated areas, respectively (field corners were not irrigated). Each half of the fields were cropped and fallowed in alternating seasons to reduce spatial variability in antecedent soil water contents, and this also may have reduced crop vulnerability to pests and diseases. Crop data used in the present study included two seasons each of conventional corn, DT corn, cotton, and grain sorghum (simply termed sorghum herein) (Table 1).

Details of each crop season are in Table 1 references, but are briefly summarized here. Crops were planted in circular raised beds spaced 0.76 m apart, and furrow dikes were installed in crop interrows following crop establishment to control runon and runoff. Irrigation water was applied in alternate interrows (i.e., drops spaced 1.52 m apart) and usually by low-energy precision application (LEPA) equipped with double-ended drag socks, although low-elevation spray application (LESA) was used in some seasons.

Table 1
Crop seasons used to test two-source energy balance model (TSEB) and additional references.

Crop		Corn[a]	Corn[a]	Corn	Corn	Cotton[b]	Cotton[c]	Sorghum[d]	Sorghum[e]
Year		2014	2014	2015	2015	2008	2013	2010	2011
Location		S PVT	S PVT	S PVT	S PVT	N PVT	N PVT	N PVT	S PVT
Cultivar		PIO 0876HR	PIO 33Y75	PIO 0157AM	PIO 9697AM	DP 117B2RF	DP 1212RFBG2	PIO 84G62	NC T5C35
Plant DOY		135	135	174	174	141	151	152	180
Harvest DOY		279	293	306	306	326	312	288	298
CGDD at harvest	(°C)	1690	1780	1650	1650	1150	1200	1460	1640
Irrigation rate	(%)	50, 75, 100	50, 75, 100	100	100	100	75	80	80
In-season *P*	(mm)	308	339	138	138	389	181	164	8
In-season *ETo*	(mm)	883	927	743	743	1010	1051	687	812
In-season *P*/*ETo*		0.35	0.37	0.19	0.19	0.39	0.17	0.24	0.010
Annual *P*	(mm)	527	527	964	964	458	284	483	170
Annual *ETo*	(mm)	1708	1708	1493	1493	1722	1836	1769	1976
Annual *P*/*ETo*		0.31	0.31	0.65	0.65	0.27	0.15	0.27	0.086

[a] Mounce et al. (2016).
[b] O'Shaughnessy and Evett (2010a), O'Shaughnessy et al. (2011a).
[c] O'Shaughnessy et al. (2015).
[d] O'Shaughnessy et al. (2012a, 2014).
[e] O'Shaughnessy et al. (2013, 2014).

Irrigation water applied was measured by calibrated totalizing flow meters. Experimental designs were typically randomized complete blocks, and experimental treatments included different irrigation rates (% of meeting full *ETc* requirements) and irrigation scheduling methods (manual by soil water profile measurement by neutron probe or automatic by T_B measurement by IRTs). Experimental plots were typically 12–18 rows wide (9–14 m, respectively) and 12–132 m long (depending on distance from pivot point) (Fig. 2).

Plant growth stages were recorded approximately weekly or biweekly in experimental plots in 1.5–2.0 m areas. These included w_C and h_C measurements, and plant population counts up to or shortly following crop establishment. A limited set of LAI measurements were obtained for one cotton season and two grain sorghum seasons. Destructive plant samples were obtained several experimental plots. Plants were placed in coolers and transported indoors, leaves were stripped from plants, and leaf area was measured by a leaf area meter (model LI-3100, LI-COR, Lincoln, Neb.) and *LAI* was determined. Calibration of the meter was checked with a 0.005 m^2 reference disk. Measured *LAI* was compared to calculated *LAI* using an allometric method based on h_C, plant population, and *CGDD* (Colaizzi et al., 2017). Because *LAI* measurements were not available for most of the crop seasons used in the present study, the allometric method was required to calculate *LAI* for plots used to test the TSEB model.

Wired and wireless IRTs were deployed on moving center pivots to measure T_B and at stationary field locations to measure T_{REF} (Fig. 2). Most data obtained prior to 2011 used wired IRTs (model IRT/c.5.1-T-80F/27C, Exergen, Inc. Watertown, Mass.) (O'Shaughnessy et al., 2012a). The wired IRT detector was a Type T (copper-constantan) thermocouple with a bandpass of 8–14 μm and reported precision and accuracy of 0.01 °C and ±0.5 °C, respectively (i.e., for a target temperature range of ±24 °C). Wireless IRTs and wireless mesh networks were developed in-house and also deployed on moving center pivots and at stationary field locations (O'Shaughnessy et al., 2013; the system was recently commercialized by Dynamax, Inc., Houston, Tex.). The wireless IRT included an infrared thermometer sensor (model MLX90614-BCF, Melexis, Ypres, Belgium) with a bandpass of 5.5–14 μm, reported precision and accuracy of 0.02 °C and ±0.5 °C, respectively, and proprietary detector temperature compensating circuitry. Both wired and wireless IRTs had approximately a 5:1 field of view (*FOV*). For each experimental plot, two moving IRTs aboard the center pivot viewed the canopy in opposite directions to average temperature differences of sunlit and shaded surfaces (Wanjura and Upchurch, 2001). Moving IRTs were placed on masts approximately 1.5 m forward of drop hoses (i.e., ahead of the center pivot direction of travel), 2.0 m above the ground (V_R), 45° zenith angle (θ_R), and 0° to 45° azimuth angle (φ_R), where 0° is perpendicular to the crop row. Three to ten stationary IRTs viewed crop rows usually at nadir, and height above ground varied with h_C. Most stationary IRTs were deployed in plots having the largest irrigation rates.

Wired and wireless IRTs were tested in a controlled temperature room (Environmental Growth Chambers, Inc., Chagrin Falls, Oh.) using a black body reference surface (model CES100, Electro Optical Industries, Inc., Santa Barbara, Calif.). O'Shaughnessy et al. (2011b) reported test results of 24 wireless IRT prototypes and compared wireless and wired IRTs in outdoor conditions. In the controlled temperature room, the black body surface temperature was varied from 15 °C to 55 °C in 5 °C increments at four ambient temperatures of 15 °C, 25 °C, 35 °C, and 45 °C, where the target and ambient temperatures were the expected ranges during a typical growing season at the study location. Without calibration, the wireless IRTs vs. black body temperature root mean squared error (RMSE) ranged from 0.13 °C to 0.37 °C (0.26 °C average), and mean bias error (MBE) ranged from −0.2 °C to 0.76 °C. After applying a linear calibration, the RMSE range was reduced only to 0.10 °C to 0.31 °C (0.18 °C average), with nearly the same MBE. Thus the RMSE range was comparable to the manufacturer-reported accuracy of ±0.5 °C with or without calibration, and the proprietary detector temperature compensation was effective for the expected ranges of target and ambient temperatures. The wireless IRTs were compared to the wired IRTs outdoors over ~48 h, which included a wide range of downwelling atmospheric longwave irradiance. The IRTs viewed a black aluminum block (81 cm × 38 cm × 7.6 cm thick) having a measured emissivity of 0.99 at near-nadir; the aluminum block was placed on a grass surface (assumed emissivity = 0.98). Therefore, a small amount of downwelling atmospheric longwave irradiance would have been reflected into the IRTs either from the aluminum block or the adjacent grass surface. The target temperatures of the aluminum block ranged from ~10 °C to 45 °C, with standard errors for wired vs. wireless IRTs ≤ 0.43 °C, slope = 1.00, and intercept = −0.25 °C, and coefficient of determination (r^2) = 0.9987.

Micrometeorological measurements required for the TSEB model were obtained at a grass reference site maintained with well-irrigated fescue at ~0.12 m height, termed the Weather Pen (WP) (Howell et al., 2000). The WP site was adjacent to and ~200 m south of the N PVT, and ~1.6 km north of the S PVT. Although micrometeorological instruments were also deployed at each center pivot, WP data were used in the TSEB model at both the N PVT and S PVT to maintain consistency. Furthermore, commercial applications are unlikely to include full agricultural meteorological stations at each center pivot. Micrometeorological variables

included incoming solar irradiance (R_S), T_A, relative humidity (RH), wind speed (U), and wind direction (φ_U). R_S was measured by a pyranometer (model PSP, Eppley Laboratories, Inc., Newport, RI), T_A and RH were measured in an enclosed ventilated white shelter at 2 m height above ground (model HMT330, Vaisala, Inc., Helsinki, Finland), U was measured by a cup anemometer at 2 m height above ground (model 03101, R.M. Young, Inc. Traverse City, Mich.), and φ_U was measured by a vane monitor at 10 m above ground (model 05103, R.M. Young, Inc. Traverse City, Mich.). Nearly all crop data had $h_C > 0.12$ m; therefore, U measured over fescue at the WP was adjusted using the logarithmic profile assumption for 2 m over cotton and sorghum and 3 m over corn (Howell, 1990). Precipitation was measured at each center pivot site by a tipping bucket rain gage (model TE525, Texas Electronics, Inc., Dallas, Tex.) and recorded by a datalogger (model CR10X, Campbell Scientific, Inc., Logan, UT). Tipping bucket rain gage measurements were sometimes verified by conventional (manual) rain gages at the center pivot locations. All micrometeorological data were screened for quality following the procedures of Allen et al. (1998).

2.5. Statistical analysis

Daily *ETc* calculated by the TSEB model and SSWB method were compared by calculating the respective means and standard deviations (*SD*), and discrepancies were quantified by the root mean square error (*RMSE*), mean absolute error (*MAE*), mean bias error (*MBE*), regression slope, regression intercept, and regression coefficient of determination (r^2), and index of model agreement (*IOA*). The *RMSE*, *MAE*, and *MBE* were also reported as percentages of mean daily SSWB *ETc*. The *IOA* is a first order version of the commonly used Coefficient of Model Efficiency (Nash and Sutcliffe, 1970), which is less sensitive to outliers (Legates and McCabe, 1999). The same statistics were also calculated for measured vs. calculated *LAI* (when data were available), and when comparing daily *ETc* measured by lysimeter to the SSWB method to facilitate comparison with results of Evett et al. (2012), where *ETc* values were cumulative over several days between neutron probe measurements. This was also done when comparing T_A at the WP and S PVT.

2.6. Sensitivity analysis

A sensitivity analysis was conducted for selected input variables deemed as having the largest uncertainty in the TSEB model for three cotton canopy sizes (small, medium, and large). Input variables were grouped by time scales (i.e., how they varied over the season), and included seasonal (essentially time invariant), daily, and diurnal. Output variables included daily E, T, and ETc. The sensitivity (S_M) of output variables (O) to input variables (I) was calculated after Oyarzun et al. (2007):

$$S_M = \frac{(O_+ - O_-)/O_B}{(I_+ - I_-)/I_B} \quad (14)$$

where I_B and O_B are the base values of input and output variables, respectively, and the + and − subscripts are the resulting values when the input variables are increased or decreased, respectively. Input variables having seasonal to daily time scales, such as IRT deployment variables and canopy size, were varied ±25% of their base values, which was deemed as characterizing their maximum uncertainty (Howell et al., 1997; Anderson et al., 2004). Input variables having diurnal time scales, such as micrometeorological variables and surface temperatures, had smaller uncertainties within approximately ±10% because these were screened for quality (e.g., Allen et al., 1998; O'Shaughnessy et al., 2011b). Uncertainties of ε_C and ε_S were deemed 0.98 ± 0.01 after Campbell and Norman (1998) and field measurements, respectively, but these were both varied from 0.90 to 1.0.

3. Results

3.1. SSWB and Kc method test

Daily *ETc* for each of the six access tubes in the NE and SE lysimeter fields was calculated by the SSWB and Kc approach, averaged, and compared with daily *ETc* measured by lysimeter (Table 2, Fig. 3). On most days, the NE lysimeter had larger *ETc* compared with *ETc* averaged from the SSWB in the NE field (means were 7.4 and 6.8 mm d^{-1}, respectively), but this was not the case for the SE lysimeter vs. the SSWB for the SE field (means were 5.7 and 6.0 mm d^{-1}, respectively). The same trends resulted in Evett et al. (2012), although scatter between lysimeter and SSWB *ETc* values was slightly smaller (see their Table 2 and Fig. 7). The larger discrepancies in the NE field were likely due to greater spatial variability of plant size during early season rapid growth. During this time, h_C (and probably *LAI*) in the NE lysimeter was larger compared with plants around the access tubes in the surrounding NE field, which corresponded to larger *ETc* in the NE lysimeter. However, h_C variability was not as large between the SE lysimeter and surrounding field, and corresponding *ETc* discrepancies were smaller. From these results, and considering that at least some discrepancies of *ETc* between lysimeters and SSWB were related to local variations in plant size, the SSWB and Kc approach were deemed suitable to estimate daily *ETc* in the center pivot experimental plots.

To further illustrate, examples of *Kc* data and their Fourier series functions were calculated for crops grown in the center

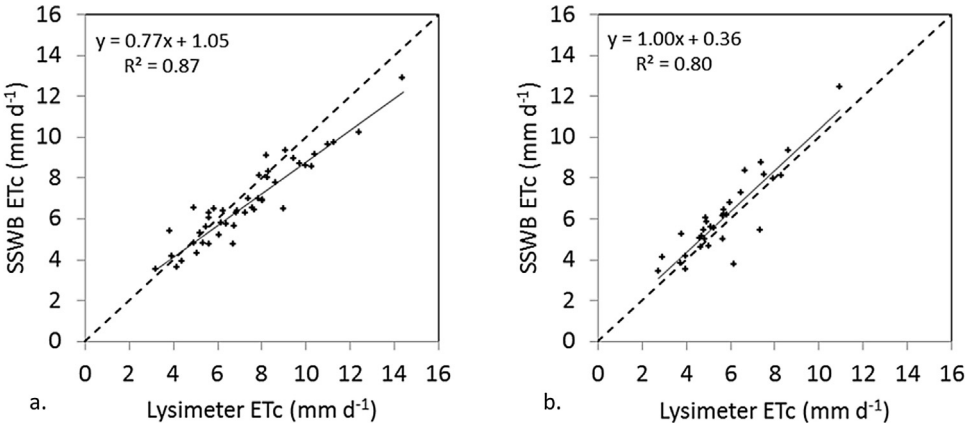

Fig. 3. Discrepancies of crop evapotranspiration (*ETc*) measured by lysimeter and calculated by a simple soil water balance (SSWB) (+ symbols), regression line (solid line), and 1:1 line (dashed line) for a. Northeast; and b. Southeast lysimeters (see Table 2 for statistics).

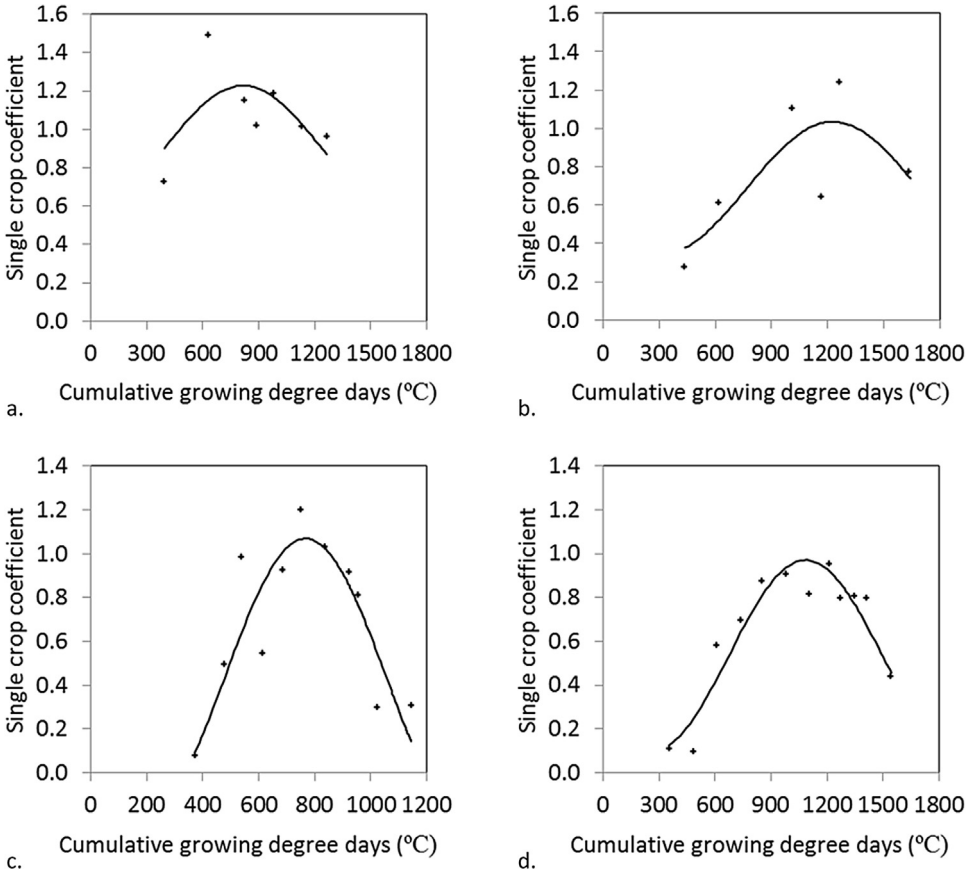

Fig. 4. Examples of plot-specific single crop coefficient models (solid line) fit to plot-specific soil water balance measurements (+ symbols) for a. conventional corn (2015 season, Plot 17, $r^2 = 0.76$, $SE_y = 0.14$); b. drought-tolerant corn (2014 season, Plot 24, $r^2 = 0.62$, $SE_y = 0.20$); c. cotton (2008 season, Plot 11, $r^2 = 0.75$, $SE_y = 0.10$); and d. grain sorghum (2011 season, Plot 28, $r^2 = 0.89$, $SE_y = 0.054$).

Table 2
Discrepancies of crop evapotranspiration (*ETc*) measured by lysimeter (Lys.) and calculated by a simple soil water balance (SSWB).

Crop		Cotton	Cotton
Year		2008	2008
Location		NE Lys.	SE Lys
n		46	33
Lys. mean	mm	7.4	5.7
Lys. *SD*	mm	2.4	1.7
SSWB mean	mm	6.8	6.0
SSWB *SD*	mm	2.0	1.9
Intercept	mm	1.1*,†	0.36*
Slope		0.77*,‡	1.00*
r^2		0.87*	0.80*
IOA		0.76	0.73
RMSE	mm	1.1	0.92
	%	15%	16%
MAE	mm	0.89	0.72
	%	12%	13%
MBE	mm	−0.63	0.37
	%	−8.5%	6.5%

* Significant ($p < 0.05$).
† Significantly different from zero ($p < 0.05$).
‡ Significantly different from unity ($p < 0.05$).

pivot fields, including conventional and drought tolerant (DT) corn varieties, cotton, and grain sorghum (Fig. 4). Peak *Kc* were larger for conventional compared with DT corn (Mounce et al., 2016). The corn crop seasons (2014 and 2015) had greater precipitation amounts compared with the cotton (2008) or sorghum (2011) seasons shown (Table 1). In fact, 2011 was the driest and 2015 was one of the wettest years on record at the study location, and this likely impacted the differences in scatter (i.e., r^2) in the different years due to uncertainty related to rainfall spatial variability and measurement error (Evett et al., 2012).

3.2. *Allometric* LAI *model test*

Discrepancies between calculated and measured *LAI* were assessed for cotton (N08 season) and grain sorghum (S10 and S11 seasons) (Table 3, Fig. 5). Overall, discrepancies were very similar to a previous study for cotton and grain sorghum, where the allometric model used to calculate *LAI* was developed and tested (Colaizzi et al., 2017). In the previous study, *LAI* measurements were also obtained at Bushland, Texas, but for crops planted in straight rows and usually irrigated by lateral move sprinklers. In the present study, *LAI* measurements were obtained from circular rows irrigated by center pivot LEPA drag socks. The similar discrepancies for the previous and present studies suggest that the allometric *LAI* model had application to different seasons, climatic, growing, and management conditions. In the present study, measured *LAI* for cotton varied from ~0.05 to 2.9 m^2 m^{-2}, and for grain sorghum, measured *LAI* varied from ~0.25 to 4.0 m^2 m^{-2}. These *LAI* measurements exemplified the range of sparse to full vegetation cover used to test the TSEB for these crops. Although *LAI* measurements were not available for corn, calculated *LAI* varied from ~0.5 to 7.0 m^2 m^{-2} (data not shown).

3.3. *TSEB model test*

Discrepancies of *ETc* calculated by the TSEB model and estimated by the SSWB method were assessed for conventional and drought

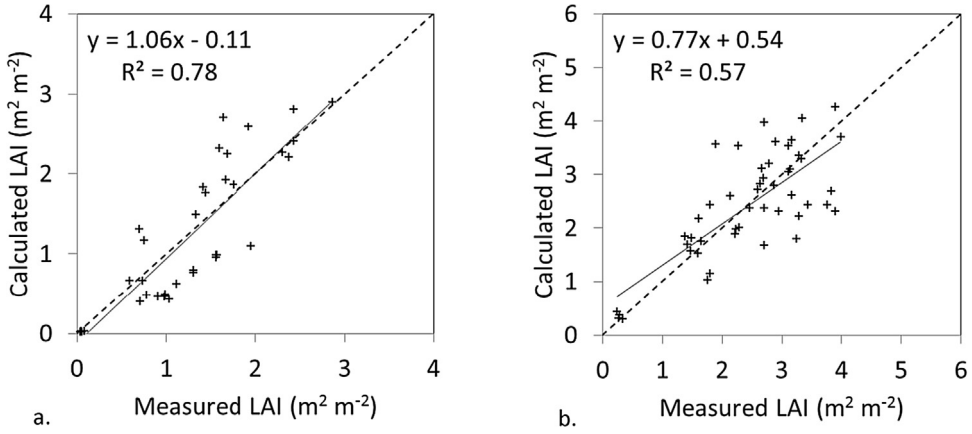

Fig. 5. Calculated vs. measured leaf area index (*LAI*) using an allometric model (+ symbols), regression line (solid line), and 1:1 line (dashed line) for a. cotton; and b. grain sorghum (see Table 3 for statistics).

Table 3
Discrepancies between calculated and measured leaf area index (*LAI*).

Crop		Cotton	Sorghum
Year		2008	2010, 2011
Location		N PVT	S PVT, N PVT
n		40	48
Meas. mean	($m^2\ m^{-2}$)	1.2	2.5
Meas. *SD*	($m^2\ m^{-2}$)	0.77	1.0
Calc. mean	($m^2\ m^{-2}$)	1.1	2.4
Calc. *SD*	($m^2\ m^{-2}$)	0.93	1.0
Intercept	($m^2\ m^{-2}$)	−0.11*,†	0.54*,†
Slope		1.06*,‡	0.77*,‡
r^2		0.78*	0.57*
IOA		0.76	0.67
RMSE	($m^2\ m^{-2}$)	0.43	0.68
	(%)	37%	28%
MAE	($m^2\ m^{-2}$)	0.34	0.51
	(%)	29%	21%
MBE	($m^2\ m^{-2}$)	−0.044	−0.022
	(%)	−3.8%	−0.89%

* Significant ($p < 0.05$).
† Significantly different from zero ($p < 0.05$).
‡ Significantly different from unity ($p < 0.05$).

tolerant corn, cotton, and grain sorghum (Table 4, Fig. 6). Discrepancies were similar for each crop season; therefore, data were pooled for both years for each crop. Overall, discrepancies were similar for each crop, which included widely varying climatic, growing, and management conditions (Baumhardt et al., 2016). The *ETc* estimated by the SSWB method varied from ~0.5 to 14 mm d^{-1} (means 5.8–7.0 mm d^{-1}). These were similar to *ETc* measured for each crop by large weighing lysimeters over a full season at the study location (Howell et al., 1997, 2004).

Mean *ETc* by the SSWB method was larger for the conventional corn variety (7.0 mm d^{-1}) compared with the DT corn variety (5.9 mm d^{-1}) (Table 4). At the study location, Mounce et al. (2016) also reported that seasonal *ETc* was larger for conventional vs. DT corn. However, mean *ETc* calculated by the TSEB model were similar (6.4 and 6.5 mm d^{-1}, respectively), and discrepancies were larger for SSWB vs. TSEB *ETc* for DT corn. For example, the respective conventional and DT *IOA* were 0.64 and 0.58; *RMSE* were 25% and 31%, *MAE* were 20% and 25%, and *MBE* were −7.3% and 11%. The similar mean *ETc* calculated by the TSEB model implied that T_R were similar for the two corn varieties, despite having different SSWB *ETc*. This was sometimes supported by pairwise comparison tests (two-tailed Student *t*-test) of simultaneous T_R measurements in conventional vs. DT plots in both the 2014 and 2015 seasons (i.e.,

Table 4
Discrepancies of crop evapotranspiration (*ETc*) calculated by a two-source energy balance (TSEB) model and simple soil water balance (SSWB), pooled for each crop.

Crop		Corn (conv.)	Corn (DT)	Cotton	Sorghum
Year		2014, 2015	2014, 2015	2008, 2013	2010, 2011
Location		S PVT	S PVT	N PVT	N PVT, S PVT
n		48	145	425	801
SSWB mean	(mm d^{-1})	7.0	5.9	5.9	5.8
SSWB *SD*	(mm $d-^{1}$)	2.8	2.1	2.3	2.1
TSEB mean	(mm d^{-1})	6.4	6.5	5.7	5.9
TSEB *SD*	(mm d^{-1})	2.1	2.2	2.2	2.0
Intercept	(mm d^{-1})	2.26*,†	2.33*,†	1.17*,†	2.66*,†
Slope		0.60*,‡	0.71*,‡	0.77*,‡	0.54*,‡
r^2		0.65*	0.47*	0.65*	0.30*
IOA		0.64	0.58	0.69	0.56
RMSE	(mm d^{-1})	1.7	1.8	1.5	1.8
	(%)	25%	31%	25%	31%
MAE	(mm d^{-1})	1.4	1.5	1.1	1.4
	(%)	20%	25%	19%	25%
MBE	(mm d^{-1})	−0.51	0.63	−0.19	0.063
	(%)	−7.3%	11%	−3.2%	1.1%

* Significant ($p < 0.05$).
† Significantly different from zero ($p < 0.05$).
‡ Significantly different from unity ($p < 0.05$).

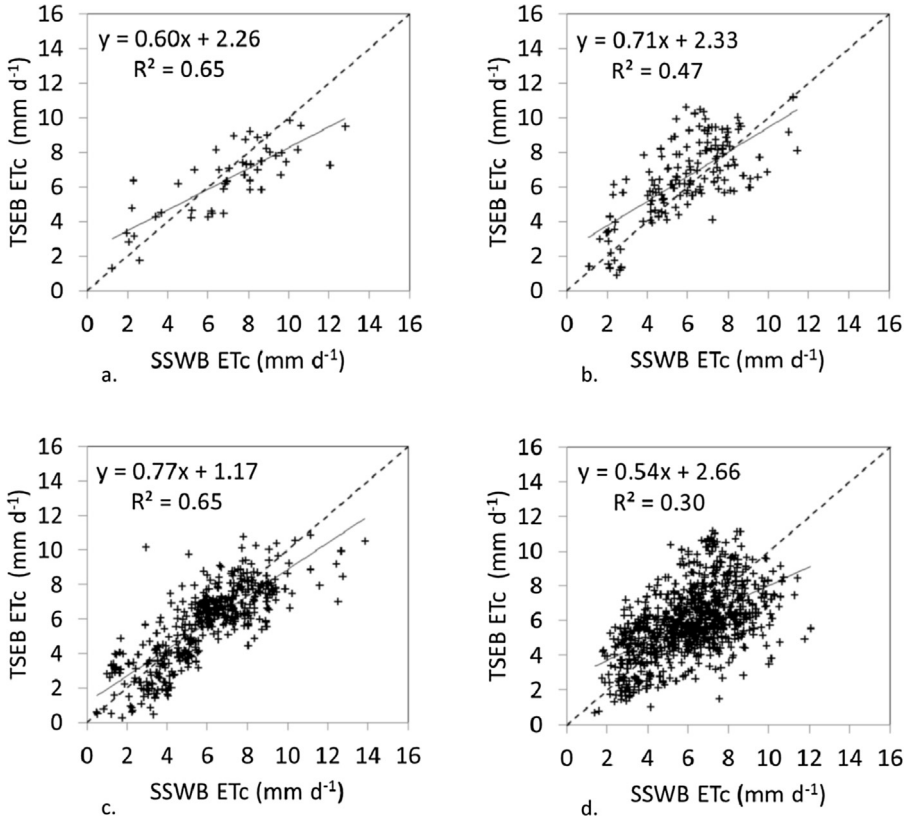

Fig. 6. Discrepancies of crop evapotranspiration (*ETc*) calculated by a two-source energy balance (TSEB) model and simple soil water balance (SSWB) (+ symbols), regression line (solid line), and 1:1 line (dashed line) for a. conventional corn; b. drought-tolerant corn; c. cotton; and d. grain sorghum (see Table 4 for statistics).

where the pivot passed through sectors having plots with both varieties with identical irrigation rates) (Fig. 7). Here, the center pivot field was divided into six pie-shaped sectors of experimental units (similar to Fig. 2). Valid comparisons were available for five and three sectors in 2014 and 2015, respectively, where each sector contained a conventional and DT plot pair with the same irrigation rate (all 100%). The pooled comparisons included most daytime hours (~0800–1700 CST), resulting in T_R (~15 °C to ~35 °C) that reflected the wide range of diurnal climatic conditions at the semi-arid study location. There was insufficient evidence to reject the null hypothesis that mean T_R were statistically equal for plot pairs in three of the five sectors in 2014 (Fig. 7a) and all three sectors in 2015 (Fig. 7b). However, two of the sectors in 2014 did exhibit evidence that T_R for the DT variety was statistically larger compared with T_R of the conventional variety (Fig. 7c and d). These exceptions clearly point to the need for a more detailed analysis of T_R and the energy balances of conventional vs. DT varieties, and will be addressed in forthcoming studies.

Mean *ETc* for cotton by the SSWB and TSEB were 5.9 and 5.7 mm d^{-1}, respectively, with most *ETc* <10 mm d^{-1}, similar to the DT corn variety (Table 4, Fig. 6). The *ETc* discrepancies for cotton were similar to the conventional corn variety, with r^2 = 0.65, *IOA* = 0.69, *RMSE* = 25%, and *MAE* = 19%, but the absolute *MBE* value was smaller compared to corn at −3.2%. Results were similar for grain sorghum, where mean SSWB and TSEB *ETc* were 5.8 and 5.9 mm d^{-1}, respectively. However, the *ETc* discrepancies were larger and similar to DT corn (except for *MBE*, which was smaller at 1.1%). The grain sorghum seasons contained two contrasting seasons (N10 and S11) (O'Shaughnessy et al., 2012b). In 2010, in-season precipitation and in-season *ETo* in 2010 were somewhat above and below average (164 and 687 mm, respectively; Table 1). The 2011 season was the driest on record, where in-season precipitation and in-season *ETo* were 8 and 812 mm, respectively (Table 1).

3.4. TSEB model sensitivity analysis

All latent heat fluxes (summed to daily *E*, daily *T*, and daily *ETc*) were most sensitive to input variables with a diurnal time scale, but less sensitive to input variables with daily or seasonal time scales (Table 5). Here, S_M of *E*, *T*, and *ETc* were denoted S_M *(E)*, S_M *(T)*, and S_M *(ETc)*, respectively. Of the diurnal input variables, latent heat fluxes were most sensitive to T_A and T_R, in most cases with $|S_M| > 1.0$ for small (DOY 201), medium (DOY 215), and large (DOY 243) canopies. Timmermans et al. (2007) also reported that *H* was more sensitive to T_R and the T_R-T_A gradient, followed by the fraction of vegetation cover, compared with other TSEB input variables. The temperature gradient-resistance relation used to calculate *H* resulted in positive correlation (shown as positive S_M) between the latent heat fluxes and T_A, but negative correlation (negative S_M) between the latent heat fluxes and T_R. Latent heat fluxes were also relatively sensitive (S_M > 1.0) to ε_C and ε_S (Table 5, Fig. 8). This was expected given that emissivity and temperature are both related to longwave flux by the Stefan-Boltzmann relation, and given the large sensitivities of latent heat fluxes to T_R. For a large canopy when the soil was obscured, the large S_M for ε_C but not ε_S was also expected. However, uncertainty in ε_C may be smaller (i.e., 0.96–0.99; Idso et al., 1969; Campbell and Norman, 1998) than the range in values shown here, which would reduce uncertainty in E, T, and ET (Fig. 8). Although ε_S may have greater uncertainty due to spatial variation of soil, and perhaps even more so due to crop residue on the surface, the impact of ε_S diminishes with increased vegetation cover. For all canopy sizes, *E* always had greater sensitivity compared with *T* or *ET* to both ε_C and ε_S. For the small and medium canopies, *E* was also relatively sensitive to R_S and *RH*. This may have been related to how the TSEB model solves the energy balance, where *E* is calculated as a residual. Somewhat surprisingly, all $|S_M| < 1.0$ for U_{-2m} and *LAI*, except for

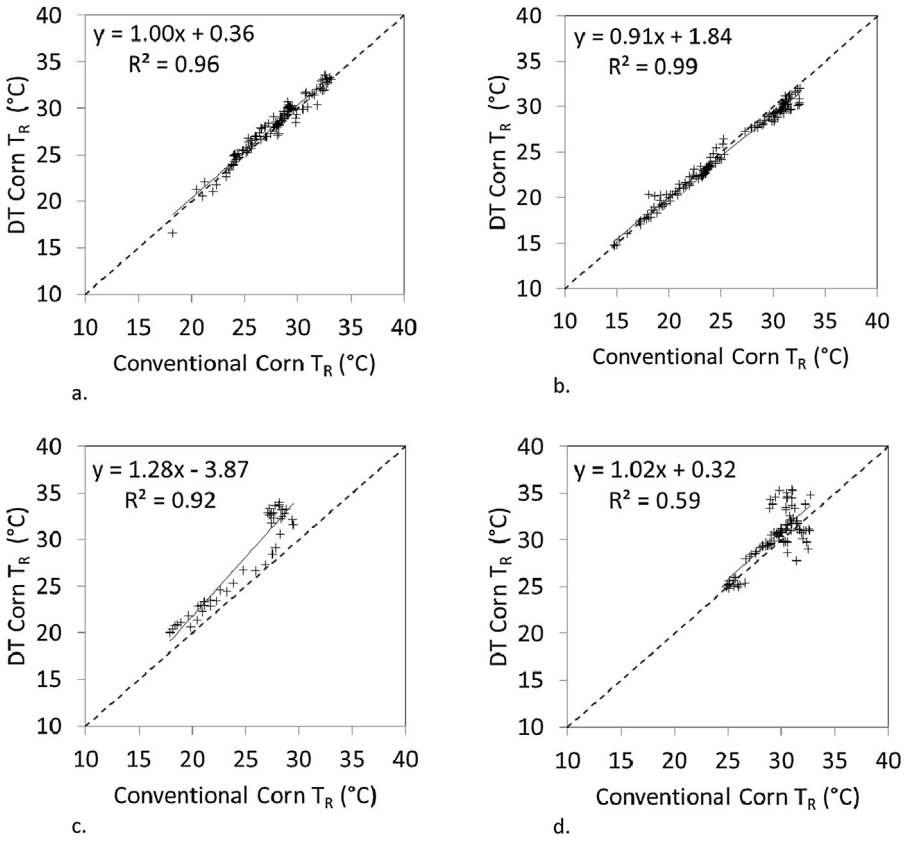

Fig. 7. Pairwise comparisons of radiometric surface temperature (T_R) between conventional and drought-tolerant (DT) corn varieties (+ symbols), regression line (solid line), and 1:1 line (dashed line) where the center pivot passed through one of six sectors (i.e., pie-shaped experimental unit) having both corn varieties with identical irrigation rates (all 100%) and identical 15-min time averages for a. 2014 Sectors 1, 2, and 3 ($p = 0.39$; $n = 121$); b. 2015 Sectors 3, 5, and 6 ($p = 0.92$; $n = 148$); c. 2014 Sector 4 ($p = 0.0012$; $n = 47$); d. 2014 Sector 6 ($p = 0.014$; $n = 90$).

Table 5
Base input (I_B) and base output (O_B) values and resulting sensitivities (S_M) of daily evaporation (E), daily transpiration (T), and daily evapotranspiration (ETc) calculated by the two-source energy balance (TSEB) model. S_M were calculated for three days from the 2008 cotton season when the canopy was small (DOY 201), medium (DOY 215), and large (DOY 243), and $|S_M| > 1.0$ are shown in bold face.

Variable[a]	Variation	DOY 201				DOY 215				DOY 243			
		I_B	O_B (E) 0.23 mm d^{-1} S_M (E)	O_B (T) 3.9 mm d^{-1} S_M (T)	O_B (ETc) 4.2 mm d^{-1} S_M(ETc)	I_B	O_B (E) 0.46 mm d^{-1} S_M (E)	O_B (T) 10.2 mm d^{-1} S_M (T)	O_B (ETc) 10.6 mm d^{-1} S_M(ETc)	I_B	O_B (E) 0.72 mm d^{-1} S_M (E)	O_B (T) 3.1 mm d^{-1} S_M (T)	O_B (ETc) 3.8 mm d^{-1} S_M(ETc)
Φ_{ROW} (°CWN)	±25%	−2	−0.13	−0.04	−0.05	−30	−0.16	−0.01	−0.02	−2	−0.01	0.03	0.02
V_R (m)	±25%	2.0	−0.14	−0.01	−0.02	2.0	−0.50	0.19	0.16	2.0	−0.08	0.02	0.00
P_R (m)	±25%	0.0	−0.29	−0.16	−0.16	0.0	0.06	−0.09	−0.09	0.0	0.12	−0.03	0.00
Θ_R (°)	±25%	45	−0.86	−0.38	−0.41	45	0.46	−0.23	−0.20	45	−0.15	0.04	0.01
Φ_R (°)	±25%	45	−0.08	−0.06	−0.06	45	−0.29	−0.03	−0.05	45	0.00	0.00	0.00
FOV	±25%	3.0	−0.11	0.01	0.01	3.0	0.21	0.08	0.09	3.0	0.00	0.00	0.00
w_C (m)	±25%	0.32	−0.07	−0.43	−0.41	0.44	0.20	−0.38	−0.36	0.48	0.41	−0.19	−0.07
h_C (m)	±25%	0.37	−0.37	−0.06	−0.07	0.66	0.15	−0.01	−0.01	0.82	0.20	0.02	0.05
LAI (m^2 m^{-2})	±25%	0.56	**−1.35**	0.11	0.03	1.66	**−1.17**	0.14	0.09	2.92	−0.30	0.09	0.02
R_S (W m^{-2})[b]	±10%	494.7	**1.67**	0.47	0.54	906.1	**1.34**	0.25	0.30	213.2	0.77	0.42	0.49
U_{-2m} (m s^{-1})[b]	±10%	4.64	−0.18	−0.01	−0.02	4.30	0.33	0.13	0.14	4.58	0.08	0.04	0.05
T_A (°C)[b]	±10%	27.6	**1.42**	**2.37**	**2.32**	33.0	**1.42**	**1.11**	**1.12**	24.5	**1.41**	**3.13**	**2.81**
RH (%)[b]	±10%	44.4	**1.40**	−0.01	0.07	29.3	0.74	0.01	0.04	59.3	0.60	−0.02	0.09
T_{REF} (°C)[b]	±10%	29.5	0.41	−0.27	−0.23	34.3	0.31	0.03	0.05	27.2	−0.18	−0.51	−0.45
T_R (°C)[b]	±10%	30.1	**−2.99**	**−2.14**	**−2.19**	27.8	**−2.70**	−0.84	−0.92	24.7	**−1.65**	**−2.74**	**−2.53**
ε_C	0.90–1.0	0.98	**1.73**	0.96	**1.00**	0.98	**2.85**	0.39	0.52	0.98	**3.35**	**2.01**	**2.23**
ε_S	0.90–1.0	0.98	**3.84**	**1.68**	**1.80**	0.98	**3.08**	−0.07	0.07	0.98	−0.15	−0.05	−0.07

[a] Φ_{ROW} (°CWN) = azimuth angle of crop row (degrees clockwise from north); V_R = vertical height of radiometer (IRT) from soil surface; P_R = perpendicular distance of IRT from crop row center; Θ_R = IRT zenith view angle; Φ_R = IRT azimuth angle to crop row (0° and 90° are parallel and perpendicular, respectively); FOV = IRT field of view; w_C = canopy width; h_C = canopy height; LAI = leaf area index; R_S = solar irradiance; U_{-2m} = wind speed measured at 2 m height, T_A = air temperature; RH = relative humidity; T_{REF} = reference temperature used in time-scaling; T_R = radiometric surface temperature; ε_C = canopy emissivity; ε_S = soil emissivity.
[b] I_B values were at solar noon (~12:45 CST).

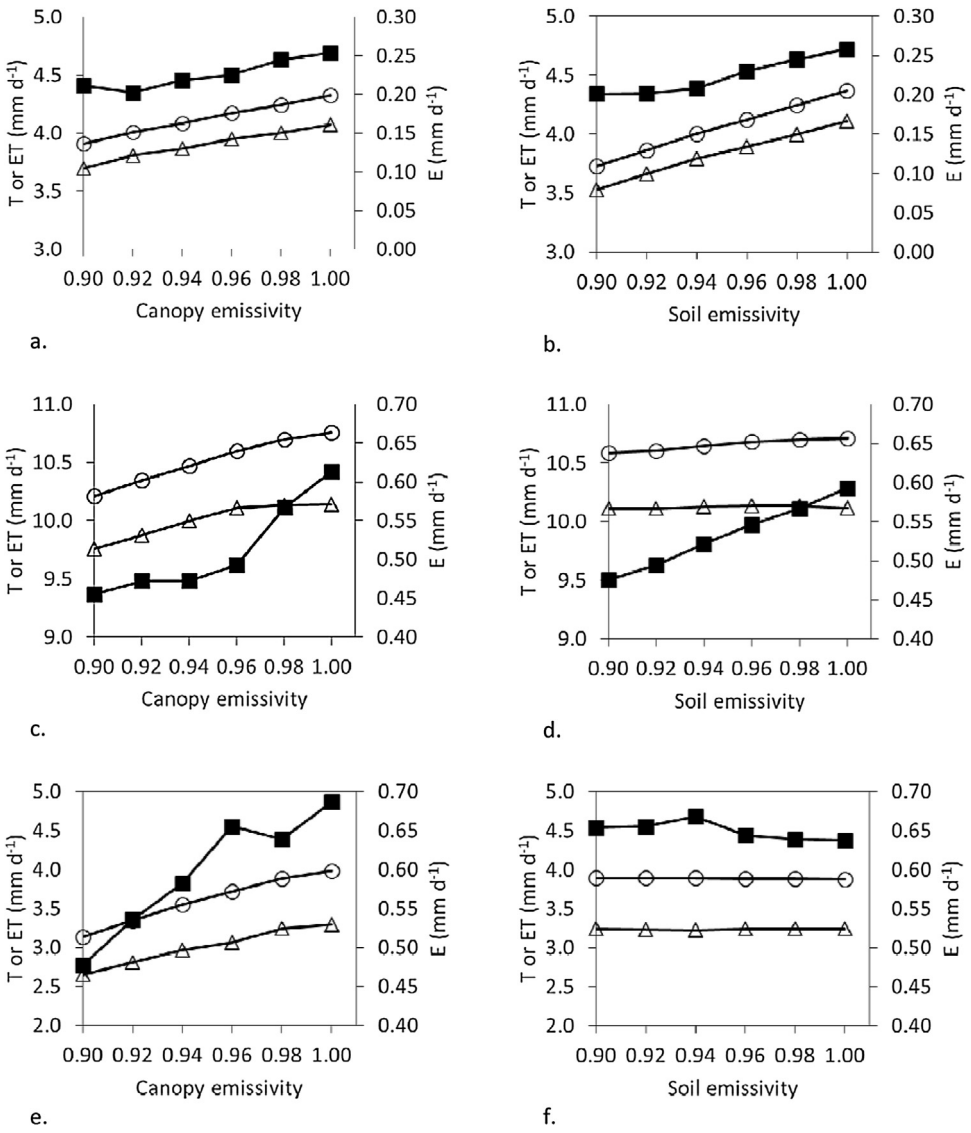

Fig. 8. Sensitivity of daily soil evaporation (E) (filled squares), daily plant transpiration (T) (open triangles), and daily evapotranspiration (ET) (open circles) calculated by the two-source energy balance (TSEB) model to canopy and soil emissivity. E, T, and ET were calculated for three days from the 2008 cotton season when the canopy was small (DOY, 201; a. and b.), medium (DOY 215; c. and d.), and large (DOY 243; e. and f.).

daily E when LAI was 0.56 m^2 m^{-2} (small canopy) or 1.66 m^2 m^{-2} (medium canopy).

The input variables considered as having seasonal time scales were related to IRT deployment (except for φ_{ROW}, which was related to center pivot angular position). Latent heat fluxes had greater sensitivities to IRT deployment variables for small and medium canopies (i.e., partial vegetation cover) compared to a large canopy (i.e., full vegetation cover). Latent heat fluxes were most sensitive to θ_R, and the largest $|S_M|$ was −0.86 for E and a small canopy, but all $|S_M| < 1.0$. The IRT deployment variables determine what fraction of vegetation appears in the IRT footprint (i.e., f_{VR}), which determines how T_R is partitioned into the canopy and soil components, and hence how E and T are partitioned in the TSEB model. The relatively low $|S_M|$ supported the generally accepted protocol for IRT deployment (Huband and Monteith, 1986; Wanjura and Upchurch, 2001), which of course seeks to maximize f_{VR}. For IRT arrays aboard center pivots, this is most practically achieved using oblique view angles to the crop row (i.e., $\theta_R = \varphi_R = 45°$) and as large V_R as practical (here, $V_R = 2.0$ m, which was larger than the 0.76-m crop row spacing).

The sensitivity analysis conducted here was to gauge the relative importance of input variables deemed to have the most uncertainty or measurement costs in the present TSEB model application. These results implied that efforts aimed at obtaining quality temperature measurements (T_A and T_R) and to a lesser extent ε_S, R_S and RH would have the largest impact on the quality of E, T, and ETc calculations using the present version TSEB model. This was congruent with previous TSEB model studies (Timmermans et al., 2007; Kustas et al., 2012), and which also motivated approaches using T_R and T_A measured at two or more times per day, such as the dual-temperature difference (DTD) algorithm (Anderson et al., 1997; Guzinski et al., 2013; Kustas et al., 2012; Norman et al., 2000). In most surface energy balance applications, however, T_A is assumed to be spatially invariable, which is likely not valid for heterogeneous landscapes (e.g., irrigated and non-irrigated areas, and even differentially irrigated plots such as those in the present study; Cammalleri et al., 2012). As discussed later, the addition of T_A (and perhaps RH) measurements to moving IRTs may well be a worthwhile area of investigation.

Input variables resulting in smaller $|S_M|$ should also be given due consideration in model applications. Note that the scope of the sen-

sitivity analysis was limited to the impact of changing one variable at a time *within the TSEB model*, and not the possible interdependence of input variables in field conditions. For example, errors in any one IRT deployment variable would not be expected to substantially contribute to error in final calculated *ETc*. But since all IRT deployment variables influence f_{VR}, small errors in more than one deployment variable may have synergistic effects and produce larger errors in final calculated fluxes in practice. Similarly, errors in *LAI* calculated by the allometric model at first may not be expected to have commensurate errors in calculated *ETc*. But *LAI* is also related to w_C and h_C, which may also have larger synergistic effects throughout the TSEB model through f_{VR}. Furthermore, the relatively small $|S_M|$ values resulting for w_C, h_C, and *LAI* were somewhat counterintuitive in light of the results of Evett et al. (2012), Timmermans et al. (2007), and data presented herein (Table 2; Fig. 3), where *ETc* was clearly impacted by differences in canopy size. On the other hand, the relatively small $|S_M|$ may have been related to the oblique IRT view angles, which resulted in larger f_{VR} compared with a nadir view, such as aerial imagery described by Timmermans et al. (2007) and French et al. (2007, 2015).

4. Discussion

Several previous studies compared latent heat flux or *ETc* calculated by the TSEB model to those measured by large weighing lysimeters and eddy covariance systems at the Bushland, TX study location. The previous studies usually resulted in smaller discrepancies between calculated and measured latent heat flux or *ETc* compared with the present study (Table 4; Fig. 6). However, the previous studies differed in several ways, perhaps most significantly because (1) ground-truth measurements were available at near instantaneous (usually 15-min) time steps and did not rely on a soil water balance or *Kc* curve fitting; (2) instruments used to measure or derive T_R were stationary (e.g., IRTs or pyrgeometers) and were not subject to uncertainty imposed by spatial variability of canopy size (i.e, w_C, h_C, or *LAI*); and (3) in most cases, other input variables such as meteorological (including precipitation) and plant measurements were obtained within a few meters of ground-truth and T_R measurements. We postulate that the larger *ETc* discrepancies reported herein were primarily related to uncertainties arising from the spatial variability and measurement error of precipitation, *LAI*, and micrometeorological variables (particularly T_A).

A brief review of previous TSEB model results at the study location follows. Kustas et al. (2012) reported *MAE* from ~10 to 20%, and *MBE* from ~1 to 5% of measured mean latent heat flux. The study considered only instantaneous fluxes and did not include time scaling to daily values. Similarly, Anderson et al. (2012) reported *MAE* ≤ 8.4% of measured means, and a Nash-Sutcliffe coefficient of model efficiency (similar to *IOA*) of ~0.92, but the study did include scaling near-instantaneous fluxes to daytime values. Although Cammalleria et al. (2014) reported *RMSE* and *MAE* of 1.8 and 1.5 mm d^{-1} between TSEB and eddy covariance derived *ETc*, which were comparable to the present study, their study derived T_R from MODIS satellite imagery having spatial resolutions much larger (~1 km) compared with the lysimeter fields (4.7 ha). Colaizzi et al. (2014) and Song et al. (2016) calculated *ETc* using several TSEB model variants and T_R derived from stationary IRTs, where near-instantaneous *ETc* calculations were summed or time scaled to daytime and 24 h values. In Colaizzi et al. (2014), the resulting calculated vs. measured *ETc* discrepancies were similar for one-time-of-day T_R measured during midday or afternoon, but larger during morning hours (13% < *RMSE* < 24%; 10% < *MAE* < 17%, and 1% < *MBE* < 10%, where percentages were of measured means). Discrepancies were similar when time scaling was not used (i.e., all 15-min T_R measurements were used over 24 h, and calculated 15-min *ETc* was summed to 24 h; *RMSE* = 12%, *MAE* = 9%, and *MBE* = 7%). Song et al. (2016) reported similar results for 24 h summed *ETc*. From these results, time scaling would not be expected to be a significant source of discrepancy between the TSEB and SSWB methods for calculating daily *ETc*, except when T_R measurements were obtained during the first half of the morning (also see Morillas et al., 2014). This is despite latent heat flux components being relatively sensitive to T_{REF} ($|S_M| > 1.0$; Table 5). The sensitivity analysis in the present study also showed large $|S_M|$ for T_R, consistent with Timmermans et al. (2007). O'Shaughnessy et al. (2011b) showed *RMSE* and *MBE* of uncalibrated wireless IRTs (used in the present study) were up to 0.79 and 1.52 °C, respectively, compared to a black body radiator in a temperature controlled room. However, wired IRTs (also used in the previous studies) showed greater discrepancy with a FLIR imager compared with wireless IRTs. Thus T_R measurement error, which could severely impact TSEB model results, would not explain smaller discrepancies reported in previous studies where wired IRTs were used.

In comparing soil water balance methods to estimate *ETc*, Evett et al. (2012) reported that accounting for vertical *F* only reduced *ETc* estimates by ~0.1 mm d^{-1}. In the present study, accounting for vertical *F* likely would have had negligible impact in reducing the TSEB vs. SSWB discrepancies (Table 4). However, uncertainties in other soil water balance components, including *I*, *P*, and *R* likely contributed to at least some discrepancies reported here (Tables 2 and 4). In particular, *P* is well known to have large spatial variability in the region, especially during summertime convective thunderstorms, which have relatively small areas (a few km) of brief but intense rainfall. Evett et al. (2012) reported a 10 mm difference in *P* between the NE and SE lysimeters (~225 m distance apart) over 132 days. However, *P* variability greater than 20 mm has been observed within a ~500 m distance and within a single day at the study location. Furthermore, *P* recorded in rain gauges has been shown to be consistently below that measured by the lysimeters due to horizontal winds and the smaller catch area (the freeboard of the lysimeter boxes prevents *R* except for the largest (>~75 mm) *P* events). Considering that the N PVT and S PVT field areas used in the present study were ~250 m and ~500 m in diameter, respectively, and each had a single rain gage at the field center, it was plausible that some discrepancy between TSEB *ETc* and SSWB *ETc* at daily time scales was caused by *P* spatial variability and measurement error of rain gages. In other studies that used soil water balances as *ETc* ground truth for a TSEB model, French et al. (2007, 2015) reported mostly smaller *RMSE* of 0.4–1.6 mm d^{-1}, where larger *RMSE* occurred after leaf senescence of spring wheat, and for one of two cotton seasons. However, *P* was likely a much smaller component of the soil water balance at their arid study location of Maricopa, Arizona (USA).

As discussed earlier, differences in *ETc* between a lysimeter and a SSWB in the surrounding field were linked to differences in canopy size, including w_C and h_C measurements, and probably *LAI* (Table 2; Fig. 3; and Evett et al., 2012). Also, previous studies having high spatial resolution reflectance measurements could detect spatial variability of vegetation cover (which presumably included differences in canopy size) on the order of a few meters (French et al., 2007; Timmermans et al., 2007). In the present study, however, measurements of w_C and h_C were available only in 1.5–2.0 m areas in each plot, requiring that *LAI* be calculated by an allometric method and also requiring the assumption that w_C, h_C, and *LAI* were uniform for each plot. Therefore, small-scale (i.e., subplot) spatial variability in canopy size was not accounted for. Given the linkage with *ETc*, the uncertainty in canopy size, especially *LAI*, may have also contributed to discrepancies of TSEB vs. SSWB *ETc*. Even if w_C, h_C, and *LAI* were available at sub-meter spatial resolution, the oblique IRT view angles likely shifted most variability in f_{VR} to earlier in the season during small or medium canopy cover, resulting in

E, *T*, and *ETc* being relatively insensitive to w_C, h_C, and *LAI* (Table 5). This was in contrast to studies using nadir views where f_{VR} would have been essentially equal to the fraction of vegetation cover throughout the season, and which resulted in relatively stronger *ETc* response to canopy cover (Anderson et al., 2005; Li et al., 2005; French et al., 2007; Timmermans et al., 2007). As an alternative to acquiring high-spatial resolution images, and to leverage existing hardware, Casanova et al. (2014) described the preliminary development of a computer vision sensor (i.e., panchromatic and reflectance imaging sensor and firmware) to be used concurrently with IRTs aboard center pivots. A field prototype remains under development, but will be tested in future studies.

Spatial variability of microclimate in heterogeneous landscapes, and their impacts on thermal-based energy balance models, has been well-documented (e.g., Cammalleri et al., 2012; Choi et al., 2009; Kustas et al., 2012; Sánchez et al., 2008). In the present study, LE fluxes (*E*, *T*, and *ETc*) were relatively sensitive to T_A and R_S regardless of canopy size ($S_M > 1.0$; Table 5). The LE fluxes were less sensitive to U_{-2m} and *RH* (although *ETo* was relatively sensitive to U_{-2m} and T_A; Porter et al., 2012; Moorhead et al., 2016). Since only WP data were used (to maintain consistency in TSEB model tests), and the WP site was ~200 m and 1.6 km from the N PVT and S PVT, respectively, microclimate spatial variability may have also contributed to some model discrepancies. A complete analysis of microclimate spatial variability at the WP, N PVT, and S PVT sites was beyond the scope of this study. However, we give a brief example by comparing T_A measurements from the WP and S PVT (Table 6; Fig. 9). Both sites used similar instruments that were shielded from radiation at 2 m height above ground (the S PVT site used model HMP45C, Vaisala, Inc., Helsinki, Finland) and averaged to 15-min. Here, we show two years that contrasted sharply in climatic conditions, including record drought in 2011, and abundant rainfall in 2015. These climatic conditions resulted from strong El Niño Southern Oscillation cycles (Baumhardt et al., 2016). For a given year, both sites had similar mean and *SD* of T_A. However, scatter between the two sites were less in 2011 compared with 2015; for example, respective *RMSE* were 1.0 and 1.9 °C. Annual *P* in the respective years was 170 and 964 mm (Table 1); the greater scatter in 2015 may have been related to spatial variability in rainfall, which resulted in locally reduced T_A. As an aside, Cammalleri et al. (2012) described an approach to calculate T_A (when measurements were missing) using imagery and an atmospheric boundary layer model, and reported similar discrepancies (~1 K) for T_A modeled and measured at micrometeorological stations. For the range of *RMSE* of T_A in the present study, and assuming the *RSME* of T_A and daily *ETc* are linearly related by S_M, then expected *RMSE* in daily *ETc* for a medium size canopy may be 3–6 mm d^{-1} (Table 5, where S_M ~3.0). This was larger than *RMSE* of daily *ETc* calculated by TSEB vs. SSWB for all crops ($1.5 \leq RMSE \leq 1.8$ mm d^{-1}; Table 4). Since *H* calculations in most soil-plant-atmosphere energy balance models are based on an air-surface temperature gradient, measurement of T_A near IRT locations (i.e., along pivot spans) warrants further investigation.

Table 6
Examples of discrepancies of air temperature (T_A) at 2 m height above ground and 15-min averages at Weather Pen (WP) and South Center Pivot (S PVT) for the two contrasting years of 2011 (record drought) and 2015 (record rainfall).

Crop		Sorghum	Corn
Year		2011	2015
Location		S PVT	S PVT
n		8691	6542
WP mean	(°C)	24.2	24.0
WP *SD*	(°C)	7.0	4.6
S PVT mean	(°C)	23.9	23.1
S PVT *SD*	(°C)	7.0	4.2
Intercept	(°C)	−0.06*	1.4*
Slope		0.99*	0.91*,†
r^2		0.99*	0.92*
IOA		0.94	0.86
RMSE	(°C)	1.0	1.9
	(%)	4.1%	8.0%
MAE	(°C)	0.74	1.4
	(%)	3.0%	5.9%
MBE	(°C)	−0.33	−0.86
	(%)	−1.4%	−3.6%

* Significant ($p < 0.05$).
† Significantly different from unity ($p < 0.05$).

5. Summary and conclusion

A recent version of a TSEB was tested where daily *ETc* was calculated for several crops and seasons in a semiarid climate (Bushland, Texas, USA). Crops included two seasons each of conventional corn, DT corn, cotton, and grain sorghum over most of the growing season (including sparse to full canopy cover). The crops were irrigated by center pivots, and T_B was measured by wired and wireless IRT arrays aboard the center pivots. Daily *ETc* calculated by the TSEB model was compared to daily *ETc* estimated by a SSWB, where the soil water profile was measured by a field-calibrated neutron probe, and daily *ETc* values were interpolated between neutron probe measurement days by fitting single crop coefficients to each plot. Discrepancies between TSEB and SSWB were similar for each crop and season,

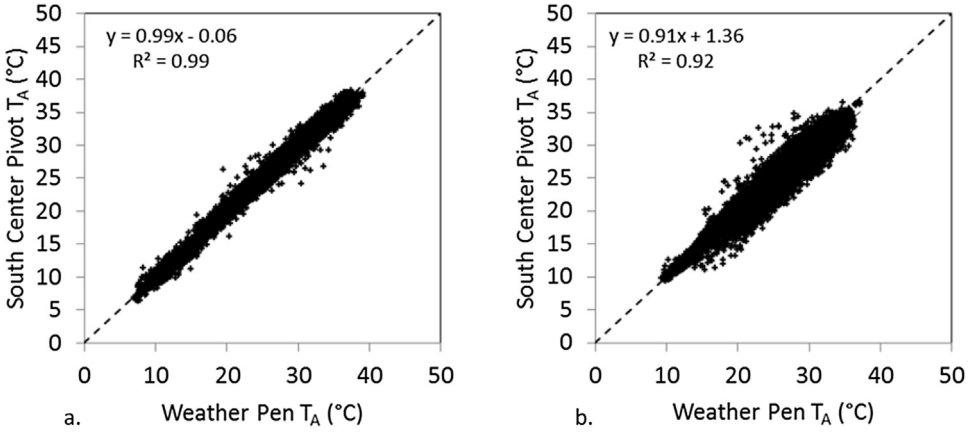

Fig. 9. Examples of discrepancies of air temperature (T_A) at 2 m height above ground and 15-min averages at Weather Pen (WP) and South Center Pivot (S PVT) (+ symbols), regression line (solid line), and 1:1 line (dashed line) for the two contrasting years of a. 2011 (record drought); and b. 2015 (record rainfall) (see Table 6 for statistics).

despite varying growing conditions primarily related to climate and management, where $0.56 \leq IOA \leq 0.69$, $1.5 \leq RMSE \leq 1.8$ mm d^{-1}; $1.1 \leq MAE \leq 1.5$ mm d^{-1}; and $-0.51 \leq MBE \leq 0.63$ mm d^{-1}.

A sensitivity analysis of daily LE components (daily *E*, daily *T*, and daily *ETc*) calculated by the TSEB model to selected input variables was conducted. Input variables having seasonal and daily time scales were varied ±25%. These variables included φ_{ROW}, IRT deployment variables (V_R, P_R, θ_R, and φ_R, and *FOV*), and canopy size (w_C, h_C, and *LAI*). Input variables having diurnal time scales were varied ±10% and included micrometeorological variables (R_S, U_{-2m}, T_A, and *RH*), and T_{REF} and T_R. In addition, ε_C and ε_S were varied from 0.90 to 1.00. The sensitivity analysis was conducted for a small, medium, and large sized cotton canopy. Daily latent heat flux components were most sensitive to T_R, T_A, and R_S for all canopy sizes, ε_S for a small canopy, and ε_C for a large canopy (i.e., most $|S_M| > 1.0$). Although each daily LE component was relatively less sensitive to canopy size, possible interdependence of input variables (e.g., w_C, h_C, and *LAI*) could enhance their impact under field conditions.

Discrepancies of daily *ETc* calculated by TSEB and SSWB were larger compared with previous TSEB model studies at this location. Based on the sensitivity analysis and previous studies, the larger discrepancies of the present study were mostly attributed to greater uncertainty of *P*, canopy size, and T_A, where uncertainties were related to both spatial variability and measurement error. Previous studies showed that *P* and canopy size impacted *ETc* estimated by the SSWB method, and canopy size and T_A impacted *ETc* calculated by the TSEB model. Although the sensitivity analysis indicated that T_R measurement error would also have a very deleterious impact in TSEB applications, calibration studies showed that wired IRTs such as those used in the previous studies were slightly less accurate compared with wireless IRTs used in the present study. Hence differences in T_R measurement error would not explain the smaller discrepancies reported in previous studies. Nonetheless, ongoing improvements in wireless IRT design are expected to reduce uncertainty in T_R measurements. Also, a computer vision sensor is presently being developed for testing at the study location to mitigate uncertainty in canopy size and T_R partitioning to the T_C and T_S components. A current field study at the N PVT site includes measurement of the 1.0-m soil water profile by time-domain reflectometry averaged to 15-min time steps, which is expected to reduce uncertainty in *ETc* estimated by soil water balance methods. Future TSEB model studies will include a larger number of rain gage and T_A sensors distributed throughout the field, along with *E* and *T* measurements by microlysimeter and sap flow gages, respectively.

Disclaimer

Mention of company or trade names is for description only and does not imply endorsement by the USDA. The USDA is an equal opportunity provider and employer.

Acknowledgements

Data presented herein was the result of numerous funding sources and dedicated efforts of technicians and student workers. Funding sources included the USDA-ARS National Program 211, Water Availability and Watershed Management; the USDA-ARS Ogallala Aquifer Program, a consortium between the USDA-ARS, Kansas State University, Texas AgriLife Research, Texas AgriLife Extension Service, Texas Tech University, and West Texas A&M University; a joint grant from the Bilateral Agricultural Research and Development (BARD) fund and the Texas Department of Agriculture (grant no. TIE04-01); a Cooperative Research and Development Agreement (CRADA) between USDA-ARS and Valmont Industries, Inc., Valley, Nebraska (Agreement No. 58-3K95-0-1455-M); and the United Sorghum Checkoff Program (grant nos. R0021-09 and R0012-10). We greatly appreciate the work performed by Luke Britten, Agricultural Science Technician, Brice Ruthhardt, Support Scientist, and the numerous temporary student workers at USDA-ARS Conservation and Production Research Laboratory, Bushland, Texas. Finally, we thank the Editor, Associate Editor, and two anonymous reviewers for their work; their comments and questions greatly improved the clarity and quality of the manuscript.

References

ASCE, 2005. The ASCE standardized reference evapotranspiration equation. In: Allen, R.G., Walter, I.A., Elliott, R.L., Howell, T.A., Itenfisu, D., Jensen, M.E., Snyder, R.L. (Eds.), ASCE-EWRI Task Committee Report. ASCE, Reston, VA.

Ahmad, M.D., Turral, H., Nazeer, A., 2009. Diagnosing irrigation performance and water productivity through satellite remote sensing and secondary data in a large irrigation system of Pakistan. Agric. Water Manage. 96, 551–564.

Alfieri, J.G., Kustas, W.P., Prueger, J.H., Hipps, L.E., Evett, S.R., Basara, J.B., Neale, C.M.U., French, A.N., Colaizzi, P., Agam, N., Cosh, M.H., Chavez, J.L., Howell, T.A., 2012. On the discrepancy between eddy covariance and lysimetry-based surface flux measurements under strongly advective conditions. Adv. Water Resour. 50, 62–78.

Allen, R.G., Pereira, L.S., Raes, D., Smith, M., 1998. Crop Evapotranspiration: Guidelines for Computing Crop Water Requirements Irrigation and Drainage Paper No. 56. United Nations FAO, Rome, Italy.

Anderson, M.C., Norman, J.M., Diak, G.R., Kustas, W.P., Mecikalski, J.R., 1997. A two-source time-integrated model for estimating surface fluxes using thermal infrared remote sensing. Remote Sens. Environ. 60, 195–216.

Anderson, M.C., Neale, C.M.U., Li, F., Norman, J.M., Kustas, W.P., Jayanthi, H., Chavez, J., 2004. Upscaling ground observations of vegetation water content, canopy height, and leaf area index during SMEX02 using aircraft and Landsat imagery. Remote Sens. Environ. 92, 447–464.

Anderson, M.C., Norman, J.M., Kustas, W.P., Li, F., Prueger, J.H., Mecikalski, J.R., 2005. Effects of vegetation clumping on two-source model estimates of surface energy fluxes from an agricultural landscape during SMACEX. J. Hydrometeorol. 6, 892–909.

Anderson, M.C., Kustas, W.P., Alfieri, J.G., Gao, F., Hain, C., Prueger, J.H., Evett, S.R., Colaizzi, P., Howell, T.A., Chavez, J.L., 2012. Mapping daily evapotranspiration at Landsat spatial scales during the BEAREX08 field campaign. Adv. Water Resour. 50, 162–177.

Anderson, R.G., Alfieri, J.G., Tirado-Corbalá, R., Gartung, J., McKee, L.G., Prueger, J.H., Wang, D., Ayars, J.E., Kustas, W.P., 2017. Assessing FAO-56 dual crop coefficients using eddy covariance flux partitioning. Agric. Water Manage. 179, 92–102.

Baumhardt, R.L., Mauget, S.A., Schwartz, R.C., Jones, O.R., 2016. El Niño Southern Oscillation effects on dryland crop production in the Texas High Plains. Agron. J. 108, 736–744.

Bellvert, J., Zarco-Tejada, P.J., Girona, J., Fereres, E., 2014. Mapping crop water stress index in a 'Pinot-noir' vineyard: comparing ground measurements with thermal remote sensing imagery from an unmanned aerial vehicle. Prec. Agric. 15, 361–376.

Berni, J.A.J., Zarco-Tejada, P.J., Sepulcre-Cantó, G., Fereres, E., Villalobos, F., 2009. Mapping canopy conductance and CWSI in olive orchards using high resolution thermal remote sensing imagery. Remote Sens. Environ. 113, 2380–2388.

Cammalleri, C., Anderson, M.C., Ciraolo, G., D'Urso, G., Kustas, W.P., La Loggia, G., Minacapilli, M., 2012. Applications of a remote sensing-based two-source energy balance algorithm for mapping surface fluxes without in situ air temperature observations. Remote Sens. Environ. 124, 502–515.

Cammalleria, C., Anderson, M.C., Gao, F., Hain, C.R., Kustas, W.P., 2014. Mapping daily evapotranspiration at field scales over rainfed and irrigated agricultural areas using remote sensing data fusion. Agric. For. Meteorol. 186, 1–11.

Campbell, G.S., Norman, J.M., 1998. An Introduction to Environmental Biophysics, 2nd ed. Springer-Verlag, New York, N.Y.

Casanova, J.J., O'Shaughnessy, S.A., Evett, S.R., Rush, C.M., 2014. Development of a wireless computer vision instrument to detect biotic stress in wheat. Sensors 14, 17753–17769.

Choi, M., Kustas, W.P., Anderson, M.C., Allen, R.G., Li, F., Kjaersgaard, J.H., 2009. An intercomparison of three remote sensing-based surface energy balance algorithms over a corn and soybean production region (Iowa, U.S.) during SMACEX. Agric. For. Meteorol. 149, 2082–2097.

Colaizzi, P.D., O'Shaughnessy, S.A., Gowda, P.H., Evett, S.R., Howell, T.A., Kustas, W.P., Anderson, M.C., 2010. Radiometer footprint model to estimate sunlit and shaded components for row crops. Agron. J. 102, 942–955.

Colaizzi, P.D., Evett, S.R., Howell, T.A., Li, F., Kustas, W.P., Anderson, M.C., 2012a. Radiation model for row crops: I. Geometric model description and parameter optimization. Agron. J. 104, 225–240.

Colaizzi, P.D., Schwartz, R.C., Evett, S.R., Howell, T.A., Gowda, P.H., Tolk, J.A., 2012b. Radiation model for row crops: II. Model evaluation. Agron. J. 104, 241–255.

Colaizzi, P.D., Kustas, W.P., Anderson, M.C., Agam, N., Tolk, J.A., Evett, S.R., Howell, T.A., Gowda, P.H., O'Shaughnessy, S.A., 2012c. Two-source energy balance

model estimates of evapotranspiration using component and composite surface temperatures. Adv. Water Resour. 50, 134–151.
Colaizzi, P.D., Agam, N., Tolk, J.A., Evett, S.R., Howell, T.A., Gowda, P.H., O'Shaughnessy, S.A., Kustas, W.P., Anderson, M.C., 2014. Two-source energy balance model to calculate E, T, and ET: comparison of Priestley-Taylor and Penman-Monteith formulations and two time scaling methods. Trans. ASABE 57, 479–498.
Colaizzi, P.D., Agam, N., Tolk, J.A., Evett, S.R., Howell, T.A., O'Shaughnessy, S.A., Gowda, P.H., Kustas, W.P., Anderson, M.C., 2016a. Advances in a two-source energy balance model: partitioning of evaporation and transpiration for cotton. Trans. ASABE 59, 181–197.
Colaizzi, P.D., Evett, S.R., Agam, N., Schwartz, R.C., Kustas, W.P., 2016b. Soil heat flux calculation for sunlit and shaded surfaces under row crops: 1. Model development and sensitivity analysis. Agric. For. Meteorol. 216, 115–128.
Colaizzi, P.D., Evett, S.R., Agam, N., Schwartz, R.C., Kustas, W.P., Cosh, M.H., McKee, L., 2016c. Soil heat flux calculation for sunlit and shaded surfaces under row crops: 2. Model test. Agric. For. Meteorol. 216, 129–140.
Colaizzi, P.D., Evett, S.R., Brauer, D.K., Howell, T.A., Tolk, J.A., Copeland, K.S., 2017. Allometric method to estimate leaf area index for row crops. Agron. J., accepted 25 Dec 2016.
Evans, R.G., Sadler, E.J., 2008. Methods and technologies to improve efficiency of water use. Water Resour. Res. 44, W00E04.
Evett, S.R., Howell, T.A., Schneider, A.D., Upchurch, D.R., Wanjura, D.F., 2000. Automatic drip irrigation of corn and soybean. In: Evans, R.G., Benham, B.L., Trooien, T.P. (Eds.), Proc. 4th Dec. Nat. Irrig. Symp. ASAE, St. Joseph, MI, pp. 401–408.
Evett, S.R., Tolk, J.A., Howell, T.A., 2003. A depth control stand for improved accuracy with the neutron probe. Vadose Zone J. 2, 642–649.
Evett, S.R., Schwartz, R.C., Howell, T.A., Baumhardt, R.L., Copeland, K.S., 2012. Can weighing lysimeter ET represent surrounding field ET well enough to test flux station measurements of daily and sub-daily ET? Adv. Water Resour. 50, 79–90.
Evett, S.R., 2008. Neutron moisture meters. In: Evett, S.R., Heng, L.K., Moutonnet, P., Nguyen, M.L. (Eds.), Field Estimation of Soil Water Content: A Practical Guide to Methods, Instrumentation, and Sensor Technology. IAEA-TCS-30. International Atomic Energy Agency, Vienna, Austria.
Falkenberg, N.R., Piccinni, G., Cothren, J.T., Leskovar, D.I., Rush, C.M., 2007. Remote sensing of biotic and abiotic stress for irrigation management of cotton. Agric. Water Manage. 87, 23–31.
French, A.N., Hunsaker, D.J., Clarke, T.R., Fitzgerald, G.J., Luckett, W.E., Pinter Jr., P.J., 2007. Energy balance estimation of evapotranspiration for wheat grown under variable management practices in central Arizona. Trans. ASABE 50, 2059–2071.
French, A.N., Alfieri, J.G., Kustas, W.P., Prueger, J.H., Hipps, L.E., Chávez, J.L., Evett, S.R., Howell, T.A., Gowda, P.H., Hunsaker, D.J., Thorp, K.R., 2012. Estimation of surface energy fluxes using surface renewal and flux variance techniques over an advective irrigated agricultural site. Adv. Water Resour. 50, 91–105.
French, A.N., Hunsaker, D.J., Thorp, K.R., 2015. Remote sensing of evapotranspiration over cotton using the TSEB and METRIC energy balance models. Remote Sens. Environ. 158, 281–294.
Gago, J., Douthe, C., Coopman, R.E., Gallego, P.P., Ribas-Carbo, M., Flexas, J., Escalona, J., Medrano, H., 2015. UAVs challenge to assess water stress for sustainable agriculture. Agric. Water Manage. 153, 9–19.
Gerik, T., Bean, B., Vanderlip, R., 2003. Sorghum Growth and Development. Texas Cooperative Extension, Rpt. B-6137. The Texas A&M University System, College Station, TX, 8 pp.
Gilmore, E.C., Rogers, J.S., 1958. Heat units as a method of measuring maturity in corn. Agron. J. 50, 611–615.
Guzinski, R., Anderson, M.C., Kustas, W.P., Nieto, H., Sandholt, I., 2013. Using a thermal-based two source energy balance model with time-differencing to estimate surface energy fluxes with day-night MODIS observations. Hydrol. Earth Syst. Sci. 17, 2809–2825.
Haberland, J.A., Colaizzi, P.D., Kostrzewski, M.A., Waller, P.M., Choi, C.Y., Eaton, F.E., Barnes, E.M., Clarke, T.R., 2010. AGIIS, Agricultural Irrigation Imaging System. Appl. Eng. Agric. 26, 247–253.
Han, S., Evans, R.G., Kroeger, M.W., 1994. Sprinkler distribution patterns in windy conditions. Trans. ASAE 37, 1481–1489.
Howell, T.A., Schneider, A.D., Dusek, D.A., Marek, T.H., Steiner, J.L., 1995. Calibration and scale performance of Bushland weighing lysimeters. Trans. ASAE 38, 1019–1024.
Howell, T.A., Steiner, J.L., Schneider, A.D., Evett, S.R., Tolk, J.A., 1997. Seasonal and maximum daily evapotranspiration of irrigated winter wheat, sorghum, and corn: Southern High Plains. Trans. ASAE 40, 623–634.
Howell, T.A., Evett, S.R., Schneider, A.D., Dusek, D.A., Copeland, K.S., 2000. Irrigated fescue grass ET compared with calculated reference grass ET. In: Evans, R.G., Benham, B.L., Trooien, T.P. (Eds.), Proc. 4th Dec. Nat. Irrig. Symp. ASAE, St. Joseph, MI, pp. 228–242.
Howell, T.A., Evett, S.R., Tolk, J.A., Schneider, A.D., 2004. Evapotranspiration of full-, deficit-irrigated, and dryland cotton on the northern Texas High Plains. J. Irrig. Drain. Eng. 130, 277–285.
Howell, T.A., 1990. Wind profile parameter estimation using MathCAD. Agron. J. 82, 1027–1030.
Huband, N.D.S., Monteith, J.L., 1986. Radiative surface temperature and energy balance of a wheat canopy: I. Comparison of radiative and aerodynamic canopy temperature. Bound. Layer Meteorol. 36, 1–17.
Hunsaker, D.J., Barnes, E.M., Clarke, T.R., Fitzgerald, G.J., Pinter Jr., P.J., 2005. Cotton irrigation scheduling using remotely sensed and FAO-56 basal crop coefficients. Trans. ASAE 48, 1395–1407.
Idso, S.B., Jackson, R.D., Ehrler, W.L., Mitchell, S.T., 1969. A method for determination of infrared emittance of leaves. Ecology 50, 899–902.
Idso, S.B., 1981. A set of equations for full spectrum and 8–14 μm and 10.5–12.5 μm thermal radiation from cloudless skies. Water Resour. Res. 17, 295–304.
Jackson, R.D., Idso, S.B., Reginato, R.J., Pinter Jr., P.J., 1981. Canopy temperature as a crop water stress indicator. Water Resour. Res. 17, 1133–1138.
Jackson, R.D., 1982. Canopy temperature and crop water stress. In: Hillel, D. (Ed.), Advances in Irrigation, vol. 1. Academic, New York, NY, pp. 43–85.
Jackson, R.D., 1984. Remote sensing of vegetation characteristics for farm management. Proc. SPIE 475, 81–96.
Jones, H.G., 2004. Irrigation scheduling: advantages and pitfalls of plant-based methods. J. Exp. Bot. 55, 2427–2436.
Kustas, W.P., Norman, J.M., 1999. Evaluation of soil and vegetation heat flux predictions using a simple two-source model with radiometric temperatures for partial canopy cover. Agric. For. Meteorol. 94, 13–29.
Kustas, W.P., Alfieri, J.G., Anderson, M.C., Colaizzi, P.D., Prueger, J.H., Evett, S.R., Neal, C.M.U., French, A.N., Hipps, L.E., Chavez, J.L., Copeland, K.S., Howell, T.A., 2012. Evaluating the two-source energy balance model using local thermal and surface flux observations in a strongly advective irrigated agricultural area. Adv. Water Resour. 50, 120–133.
Kustas, W.P., Nieto, H., Morillas, L., Anderson, M.C., Alfieri, J.G., Hipps, L.E., Villagarcía, L., Domingo, F., Garcia, M., 2016. Revisiting the paper Using radiometric surface temperature for surface energy flux estimation in Mediterranean drylands from a two-source perspective. Remote Sens. Environ. (in press).
Legates, D.R., McCabe Jr., G.J., 1999. Evaluating the use of goodness-of-fit measures in hydrologic and hydroclimatic model validation. Water Resour. Res. 35, 233–241.
Li, F., Kustas, W.P., Prueger, J.H., Neal, C.M.U., Jackson, T.J., 2005. Utility of remote sensing-based two-source energy balance model under low- and high-vegetation cover conditions. J. Hydrometeorol. 6, 878–891.
Li, H., Payne, W.A., Michels, G.J., Rush, C.M., 2008. Reducing plant abiotic and biotic stress: drought and attacks of greenbugs, corn leaf aphids and virus disease in dryland sorghum. Environ. Exp. Bot. 63, 305–316.
Liu, S.M., Xu, Z.W., Wang, W.Z., Jia, Z.Z., Zhu, M.J., Bai, J., Wang, J.M., 2011. A comparison of eddy covariance and large aperture scintillometer measurements with respect to the energy balance closure problem. Hydrol. Earth Syst. Sci. 15, 1291–1306.
Maes, W.H., Steppe, K., 2012. Estimating evapotranspiration and drought stress with ground-based thermal remote sensing in agriculture: a review. J. Exp. Bot. 63, 4671–4712.
McMaster, G.S., Wilhelm, W.W., 1997. Growing degree-days: one equation, two interpretations. Agric. For. Meteorol. 87, 291–300.
Moore, B.C., Coleman, A.M., Wigmosta, M.S., Skaggs, R.L., Venteris, E.R., 2015. A high spatiotemporal assessment of consumptive water use and water scarcity in the conterminous United States. Water Resour. Manage. 29, 5185–5200.
Moorhead, J.E., Gowda, P.H., Marek, G.W., Porter, D.O., Marek, T.H., 2016. Spatial uniformity in sensitivity coefficient of reference ET in the Texas High Plains. Appl. Eng. Agric. 32, 263–269.
Moran, M.S., Clarke, T.R., Inoue, Y., Vidal, A., 1994. Estimating crop water deficit using the relation between surface-air temperature and spectral vegetation index. Remote Sens. Environ. 49, 246–263.
Morillas, L., García, M., Nieto, H., Villagarcía, L., Sandholt, I., Gonzalez-Dugo, M.P., Zarco-Tejada, P.J., Domingo, F., 2013. Using radiometric surface temperature for surface energy flux estimation in Mediterranean drylands from a two-source perspective. Remote Sens. Environ. 136, 234–246.
Morillas, L., Villagarcía, L., Domingo, F., Nieto, H., Uclés, O., García, M., 2014. Environmental factors affecting the accuracy of surface fluxes from atwo-source model in Mediterranean drylands: upscaling instantaneous to daytime estimates. Agric. For. Meteorol. 189–190, 140–158.
Mounce, R.B., O'Shaughnessy, S.A., Blaser, B.C., Colaizzi, P.D., Evett, S.R., 2016. Crop response of drought-tolerant and conventional maize hybrids in a semiarid environment. Irrig. Sci. 34, 231–244.
Nash, J.E., Sutcliffe, J.V., 1970. River flow forecasting through conceptual models: part 1. A discussion of principles. J. Hydrol. 10, 282–290.
Norman, J.M., Becker, F., 1995. Terminology in thermal infrared remote sensing of natural surfaces. Remote Sens. Rev. 12, 159–173.
Norman, J.M., Kustas, W.P., Humes, K.S., 1995. Source approach for estimating soil and vegetation energy fluxes in observations of directional radiometric surface temperature. Agric. For. Meteorol. 77, 263–293.
Norman, J.M., Kustas, W.P., Prueger, J.H., Diak, G.H., 2000. Surface flux estimation using radiometric temperature: a dual temperature difference method to minimize measurement errors. Water Resour. Res. 36, 2263–2274.
O'Shaughnessy, S.A., Evett, S.R., 2010a. Canopy temperature based system effectively schedules and controls center pivot irrigation of cotton. Agric. Water Manage. 97, 1310–1316.
O'Shaughnessy, S.A., Evett, S.R., 2010b. Developing wireless sensor networks for monitoring crop canopy temperature using a moving sprinkler system as a platform. Appl. Eng. Agric. 26 (2), 331–341.
O'Shaughnessy, S.A., Evett, S.R., Colaizzi, P.D., Howell, T.A., 2011a. Using radiation thermography and thermometry to evaluate crop water stress in soybean and cotton. Agric. Water Manage. 98, 1523–1535.

O'Shaughnessy, S.A., Hebel, M.A., Evett, S.R., Colaizzi, P.D., 2011b. Evaluation of a wireless infrared thermometer with a narrow field of view. Comput. Electron. Agric. 76, 59–68.
O'Shaughnessy, S.A., Evett, S.R., Colaizzi, P.D., Howell, T.A., 2012a. A crop water stress index and time threshold for automatic irrigation scheduling of grain sorghum. Agric. Water Manage. 107, 122–132.
O'Shaughnessy, S.A., Evett, S.R., Colaizzi, P.D., Howell, T.A., 2012b. Grain sorghum response to irrigation scheduling with the time-temperature threshold method and deficit irrigation levels. Trans. ASABE 55 (2), 451–461.
O'Shaughnessy, S.A., Evett, S.R., Colaizzi, P.D., Howell, T.A., 2013. Wireless sensor network effectively controls center pivot irrigation of sorghum. Appl. Eng. Agric. 29 (6), 853–864.
O'Shaughnessy, S.A., Evett, S.R., Colaizzi, P.D., Tolk, J.A., Howell, T.A., 2014. Early and late maturing grain sorghum under variable climatic conditions in the Texas High Plains. Trans. ASABE 57 (6), 1583–1594.
O'Shaughnessy, S.A., Evett, S.R., Colaizzi, P.D., 2015. Dynamic prescription maps for site-specific variable rate irrigation of cotton. Agric. Water Manage. 159, 123–138.
Osroosh, Y., Peters, R.T., Campbell, C.S., Zhang, Q., 2015. Automatic irrigation scheduling of apple trees using theoretical crop water stress index with an innovative dynamic threshold. Comput. Electron. Agric. 188, 193–203.
Oyarzun, R.A., Stöckle, C.O., Whiting, M.D., 2007. A simple approach to modeling radiation interception by fruit-tree orchards. Agric. For. Meteorol. 142, 12–24.
Peng, S., Krieg, D.R., Hicks, S.K., 1989. Cotton lint yield response to accumulated heat units and soil water supply. Field Crops Res. 19, 253–262.
Peters, R.T., Evett, S.R., 2004. Modeling diurnal canopy temperature dynamics using one-time-of-day measurements and a reference temperature curve. Agron. J. 96, 1553–1561.
Peters, R.T., Evett, S.R., 2008. Automation of a center pivot using the temperature-time-threshold method of irrigation scheduling. J. Irrig. Drain. 134, 286–291.
Phene, C.J., Howell, T.A., Sikorski, M.D., 1985. A traveling trickle irrigation system. In: Hillel, D. (Ed.), Advances in Irrigation, vol. 3. Academic, Orlando, FL, pp. 1–49.
Playán, E., Salvador, R., Faci, J.M., Zapata, N., Martínez-Cob, A., Sánchez, I., 2005. Day and night wind drift and evaporation losses in sprinkler solid-sets and moving laterals. Agric. Water Manage. 76, 139–159.
Porter, D.O., Gowda, P.H., Marek, T.H., Howell, T.A., Moorhead, J.E., Irmak, S., 2012. Sensitivity of grass and alfalfa reference evapotranspiration to weather station sensor accuracy. Appl. Eng. Agric. 28, 543–549.
Sánchez, J.M., Kustas, W.P., Caselles, V., Anderson, M.C., 2008. Modelling surface energy fluxes over maize using a two-source patch model and radiometric soil and canopy temperature observations. Remote Sens. Environ. 112, 1130–1143.
Sadler, E.J., Camp, C.R., Evans, D.E., Millen, J.A., 2002. Corn canopy temperatures measured with a moving infrared thermometer array. Trans. ASAE 45, 581–591.
Schneider, A.D., Howell, T.A., 2000. Surface runoff due to LEPA and spray irrigation of a slowly permeable soil. Trans. ASAE 43, 1089–1095.
Senay, G.B., Budde, M.E., Verdin, J.P., Rowland, J., 2009. Estimating actual evapotranspiration from irrigated fields using a simplified surface energy balance approach. In: Thenkabail, P.S., Lyon, J.G., Turral, H., Biradar, C.M. (Eds.), Remote Sensing of Global Croplands for Food Security. CRC Press, Boca Raton, FL, pp. 317–330.
Slack, D.C., Martin, E.C., Sheta, A.E.A., Fox Jr., F., Clark, L.J., Ashley, R.O., 1996. Crop coefficients normalized for climatic variability with growing degree days. In: Camp, C.R., Sadler, E.J., Yoder, R.E. (Eds.), Proc. Int. Conf. Evapotranspiration and Irrigation Scheduling. San Antonio, TX, 3–6 Nov 1996. ASAE, St. Joseph, MI, pp. 892–898.
Song, L., Kustas, W.P., Liu, S., Colaizzi, P.D., Nieto, H., Xu, Z., Mae, Y., Li, M., Xu, T., Agam, N., Tolk, J.A., Evett, S.R., 2016. Applications of a thermal-based two-source energy balance model using Priestley-Taylor approach for surface temperature partitioning under advective conditions. J. Hydrol. 540, 574–587.
Steiner, J.L., Kanemasu, E.T., Clark, R.N., 1983. Spray losses and partitioning of water under a center pivot sprinkler system. Trans. ASAE 26, 1128–1134.
Thomasson, J.A., Shi, Y., Olsenholler, J., Valasek, J., Murray, S.C., Bishop, M.P., 2016. Comprehensive UAV agricultural remote-sensing research at Texas A M University. In: Valasek, J., Thomasson, J.A. (Eds.), Proc. SPIE 0277-786X, 9866, Autonomous Air and Ground Sensing Systems for Agricultural Optimization and Phenotyping. 986602, Baltimore, MD, 17 May 2016.
Timmermans, W.J., Kustas, W.P., Anderson, M.C., French, A.N., 2007. An intercomparison of the surface energy balance algorithm for land (SEBAL) and the two-source energy balance (TSEB) modeling schemes. Remote Sens. Environ. 108, 369–384.
Todd, R.W., Evett, S.R., Howell, T.A., 2000. The Bowen ratio energy balance method for estimating latent heat flux of irrigated alfalfa evaluated in a semi-arid, advective environment. Agric. For. Meteorol. 103, 335–348.
Tolk, J.A., Evett, S.R., 2012. Lower limits of crop water use in three soil textural classes. SSSAJ 76, 607–616.
USDA-NASS, 2014. Farm and Ranch Irrigation Survey (2013), Vol. 3, Special Studies, Part 1. USDA National Agricultural Statistics Service, Washington, D.C, Available at: https://www.agcensus.usda.gov/Publications/2012/Online_Resources/Farm_and_Ranch_Irrigation_Survey/ (Accessed 30 August 2016).
USDA-NRCS, 2016. Soil Survey TX375: Potter County Texas. USDA Natural Resources Conservation Service, Washington, D.C, Available at: http://websoilsurvey.nrcs.usda.gov (Accessed 30 August 2016).
Upchurch, D.R., Wanjura, D.F., Burke, J.J., Mahan, J.R., 1996. Biologically-Identified Optimal Temperature Interactive Console (BIOTIC) for managing irrigation. U.S. Patent No. 5539637.
Wanjura, D.F., Upchurch, D.R., 2001. Infrared thermometer calibration and viewing method effects on canopy temperature measurement. Agric. For. Meteorol. 55, 309–321.
Wanjura, D.F., Upchurch, D.R., Mahan, J.R., 1992. Automated irrigation based on threshold canopy temperature. Trans. ASAE 35, 153–159.
Woldt, W.E., Frew, E.W., Stachura, M., Smith, J., Mack, J., 2015. Conducting unmanned aircraft flight operations under Federal Aviation Administration regulations. In: ASABE Paper No. 152147654, Annual International Meeting, New Orleans, LA, 26–29 Jul 2015. ASABE: St. Joseph, MI.
Zarco-Tejada, P.J., González-Dugo, V., Williams, L.E., Suárez, L., Berni, J.A.J., Goldhamer, D., Fereres, E., 2013. A PRI-based water stress index combining structural and chlorophyll effects: assessment using diurnal narrow-band airborne imagery and the CWSI thermal index. Remote Sens. Environ. 138, 38–50.
Zwart, S.J., Bastiaanssen, W.G.M., 2007. SEBAL for detecting spatial variation of water productivity and scope for improvement in eight irrigated wheat systems. Agric. Water Manage. 89, 287–296.